



## Sinkholes, stream channels and base-level fall: a 50-year record of spatio-temporal development on the eastern shore of the Dead Sea

Robert A. Watson<sup>1</sup>, Eoghan P. Holohan<sup>1</sup>, Djamil Al-Halbouni<sup>2</sup>, Leila Saberi<sup>3</sup>, Ali Sawarieh<sup>4</sup>, Damien Closson<sup>5</sup>, Hussam Alrshdan<sup>4</sup>, Najib Abou Karaki<sup>6\*</sup>, Christian Siebert<sup>7</sup>, Thomas R. Walter<sup>2</sup>, & Torsten Dahm<sup>2</sup>

<sup>1</sup> UCD School of Earth Sciences, University College Dublin, Dublin, Ireland

<sup>2</sup> Helmholtz Centre Potsdam (GFZ), Section 2.1, Potsdam, Germany

<sup>3</sup> University of Minnesota, Department of Earth Sciences, Minneapolis, USA

<sup>4</sup> Ministry of Energy & Mineral Resources, Amman, Jordan

<sup>5</sup> Geographic Information Management, Brussels, Belgium

<sup>6</sup> Department of Environmental and Applied Geology, University of Jordan, Amman, 11942, Jordan

\*On sabbatical leave at the Environmental Engineering Department, Al-Hussein bin Talal University, Ma'an-Jordan.

<sup>7</sup> Helmholtz Centre for Environmental Research – UFZ, T. Lieser Str. 4, Halle 06120, Germany

*Correspondence to:* Eoghan P. Holohan (eoghan.holohan@ucd.ie)

**Abstract.** The fall of hydrological base-level is long established as a driver of geomorphological change in both fluvial and karst systems, but few natural occurrences occur on timescales suitable for direct observation. Here we document the spatiotemporal development of fluvial and karstic landforms along the eastern coast of the hypersaline Dead Sea (at Ghor al-Haditha, Jordan) during a 50-year period of regional base-level decline from 1967 to 2017. Combining remote sensing data with close-range photogrammetric surveys, we show that the 35 m base-level fall has caused shoreline retreat of up to 2.5 km, and resulted in: (1) incision of new meandering or straight/braided stream channels and (2) formation of >1100 sinkholes and several salt-karst uvalas. Both alluvial incision and karst-related subsidence represent significant hazards to local infrastructure. The development of groundwater-fed meandering stream channels is in places interlinked with that of the sinkholes and uvalas. Moreover, active areas of channel incision and sinkhole development both migrate seaward in time, broadly in tandem with shoreline retreat. Regarding theoretical effects of base-level fall, our observations show some deviations from those predicted for channel geometry, but are remarkably consistent with those for groundwater-



related salt karstification. Our results present, for the first time in the Dead Sea region, the dual response of surface and subsurface hydrological systems to base level drop as indicated by fluvial and karst geomorphological analysis.

## 1 Introduction

35 The concept of hydrological base-level is over 100 years old (Davis, 1902), and it is key to understanding changes of the Earth's surface due to tectonic deformation or climate change (Allen, 2008; Best and Ashworth, 1997; Whittaker, 2012). The exact definition of base-level varies between disciplines, however. In fluvial geomorphology, base level is defined as the “imaginary horizontal level to which sub-aerial erosion proceeds” (Schumm, 1993), generally regarded as sea-level. In karst geomorphology, base-  
40 level is defined as “the point of groundwater outflow from the subsurface karst drainage system” (Bakalowicz, 2005).

Regardless of definition, the rise or fall of hydrological base level is long known to result in complex geomorphological responses. Changes in fluvial channel morphology have been proposed to depend on  
45 the rate and magnitude of base level fall, the local relief and hydrological input, and the character of the channel substrate (Leopold and Bull, 1979; Schumm, 1993; Whittaker and Boulton, 2012). In a karst system, base level fall (i.e. decline in the level of the phreatic zone) is envisaged to cause new conduit development (by vadose incision and/or phreatic passage formation at the newly defined base level) and to generate new outflow points (Bakalowicz, 2005; Farrant and Simms, 2011; Ford and Williams, 2007).  
50 Subsequent karstic development may be expressed at the surface by new or accelerated formation of *dolines*, or sinkholes (as we shall refer to them) (Gutiérrez et al., 2014).

The hypersaline Dead Sea represents a regional hydrological base level that has fallen, largely because of anthropogenic-forcing, at a gradually increasing rate since the late 1960s (Lensky et al., 2005). The base  
55 level fell at a rate of 0.5 m yr<sup>-1</sup> in the 1970's, and at a rate of 1.1 m yr<sup>-1</sup> in the last decade. In absolute terms, the lake level has declined by 37 m as of 2017 and is forecast to drop a further 25-70 m by 2100 (Asmar and Ergenzinger, 2002; Yechieli and Gavrieli, 1998). The margins of the Dead Sea are undergoing



dramatic geomorphological changes including enhanced stream and river channel incision (Bowman et al., 2010; Moshe et al., 2008; Vachtman and Laronne, 2013), slope instability and landslides (Closson et al., 2010), as well as the development of several thousands of sinkholes by karstification of salt-rich deposits underlying the lake margins (Abelson et al., 2017; Yechieli et al., 2006). These changes represent substantial geohazards in the Dead Sea region. They have already destroyed or damaged tourism facilities, factories, evaporation pond dykes, highways, link roads, houses and farmland.

While geomorphological changes have been documented in some detail on the western side of the Dead Sea, less information is available about such changes on the eastern side. In this paper, we provide a first detailed documentation of the geomorphological evolution of the main sinkhole-affected site on the eastern shore of the Dead Sea, at Ghor al-Haditha in Jordan, over the 50-year period from the start of the base level drop in 1967 to 2017. Our aims are to discern factors controlling the evolution of the new landforms, and to examine how hydrological or karstic aspects interact in the context of the base-level fall.

## 2 Tectonic setting and geological framework

The Dead Sea is the hyper-saline terminal lake of the Jordan River (**Figure 1A**), and it lies within the ~150 km long and ~ 8 - 10 km wide Dead Sea basin (Garfunkel and Ben-Avraham, 1996). The basin lies at a left step (or bend) along the left-lateral Dead Sea Transform fault system. Maximum tectonic subsidence is ~8.5 km around the Lisan peninsula (Ten Brink and Flores, 2012). The basin has hosted several palaeo-lakes of varying size and duration (Bartov et al., 2002; Torfstein et al., 2009). A high-stand of -162 m elevation (with respect to modern global mean sea level, the convention used hereafter) was reached at around 25 ka ago, during the ‘Lisan Lake’ episode, and the modern Dead Sea initiated after a major low-stand at around 10 ka ago (Bartov et al., 2002). With the lake’s decline from -395 m (1967) to -431 m (2017) it has divided into northern and southern parts; the latter is now taken over by industrial salt evaporation ponds.



85 The Ghor al-Haditha study area, which is about 25 km<sup>2</sup> in size, is situated on the southeast shore of the northern Dead Sea (**Figure 1A**). The area lies in a zone of tectonic complexity at the eastern basin margin, where subsidence is relayed between several major tectonic structures along a ~ 15° bend in the Dead Sea Transform system. The major, left-lateral, N24°-trending Wadi Araba fault terminates a few kilometres south of the area, further north of which basin subsidence is accommodated by combination of the N0°-trending Ghor Safi fault and the Ed-Dhira monoclinical flexure. The Ghor Safi fault also forms the eastern  
90 boundary of the actively rising Lisan salt diapir (Al-Zoubi and Ten Brink, 2001; Fiaschi et al., 2017). The Ed-Dhira monocline terminates against the right-lateral N80°-trending Siwaqa fault, which also down-throws to the north. Further north again, a N10°-trending escarpment probably reflects the orientation of another major basin-bounding fault (Khalil, 1992), although the exact location of the fault trace is unclear.

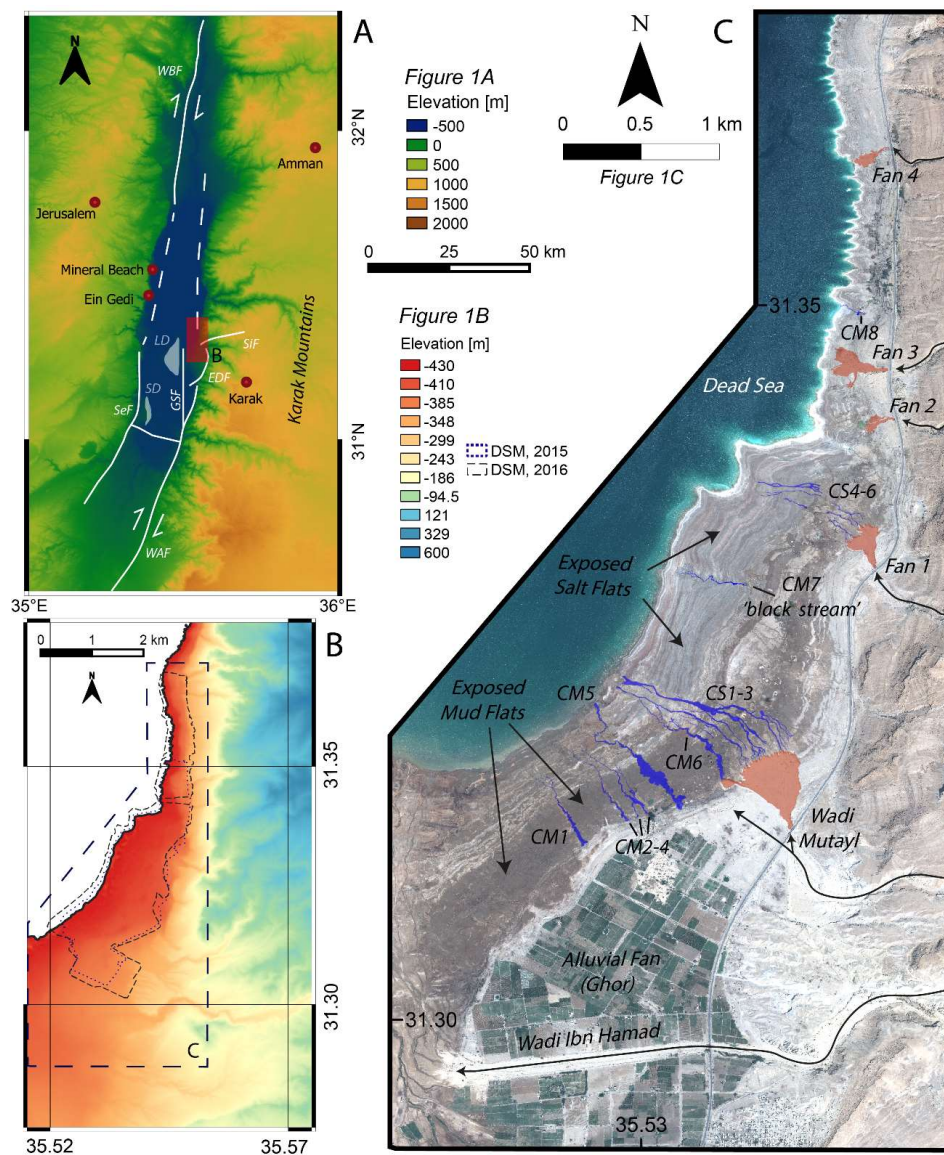
95 The geology of the Ghor al-Haditha study area comprises folded and faulted sequences of siliciclastic or carbonate rocks, which are locally overlain by semi-consolidated to unconsolidated lacustrine or alluvial deposits (**Figure 2**). Hydrogeologically, there three principal aquifer units: (1) a lower sandstone aquifer comprising the Ram group and Kurnub formation of Cambrian to early Cretaceous ages, respectively; (2) an upper carbonate aquifer spanning the Ajlun and Belqa groups of late Cretaceous to early Tertiary age;  
100 and (3) a superficial aquifer in the Lisan formation of Plio-Pleistocene age (Khalil, 1992).

The Lisan formation deposits at Ghor al-Haditha comprise poorly-sorted, semi-consolidated to unconsolidated sands and gravels interbedded with minor silts and clays. These deposits, together with similar but unconsolidated deposits of the Ze'elim formation of Holocene age, form an alluvial fan plain  
105 at between -360m and -380m (**Figure 1B, 1C**). Three major *wadi* (dry river valley) systems terminate within or adjacent to the study area: Wadi Ibn Hammad, Wadi Mutayl and Wadi al Mazra'a (the latter lies just outside the study area to the southwest). These drain the uplands to the east and southeast.

The Lisan and Ze'elim formations also comprise lacustrine deposits, some of which are exposed on the former Dead Sea bed. These form a 'mudflat' or 'saltflat' adjacent the Dead Sea shore (**Figure 1C**), and  
110 comprise laminated to thinly bedded layers of marl, clay, salt and silt interbedded with a spatially variable

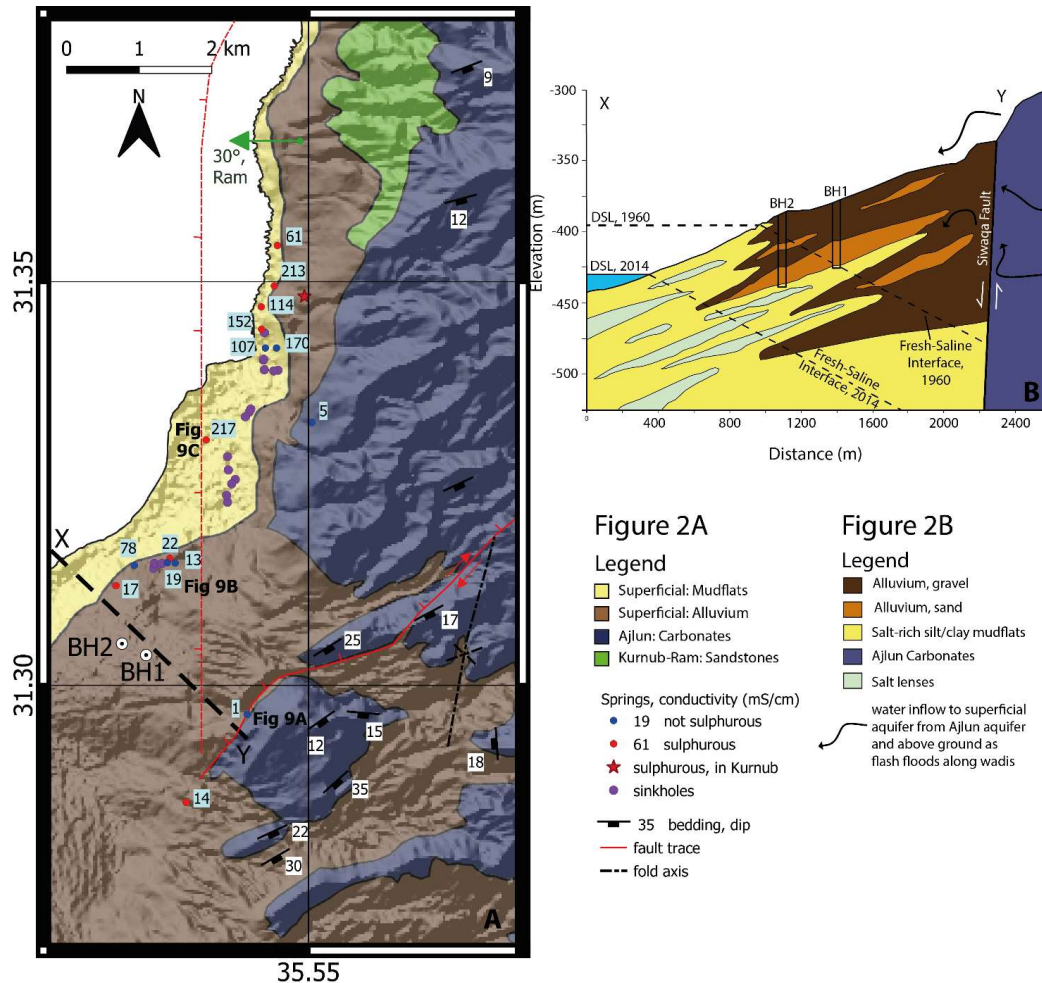


proportion of thin to thick layers of rock salt (predominantly halite). Similar lacustrine deposits likely extend in under the alluvial fan (Polom et al., 2018).





115 Figure 1: overview of the Ghor al-Haditha study area. (A) Advanced Land Observing Satellite (ALOS) 30m Digital Surface Model (DSM) of the Dead Sea study area, showing the regional tectonic regime. WBF: Western Boundary Fault; SiF: Siwaqa Fault; LD: Lisan Diapir; EDF: Ed Dhira Flexure; GSF: Ghor Safi Fault; SD: Sedom Diapir; SeF: Sedom Fault; WAF: Wadi Araba Fault. (B) ALOS 30m DSM showing relief in the study area, as highlighted in red in (A), along with the footprints of the 2015 and 2016 drone and field surveys. (C) Pleiades 2017 satellite image of the study area showing main hydrological and geomorphic features referred to later in the study.



125 Figure 2: structural and hydrogeological characteristics of the study area. (A) simplified geological map of the study area, partly based on 1:50,000 scale mapping of Jordanian Ministry of Energy and Mineral Resources (Khalil, 1992) and partly on our own work. The stratigraphy generally dips acutely to the southeast, while striking to the northeast. Also shown is the right-lateral oblique Siwaqa fault, the inferred continuation of the Dead Sea Transform (down-throwing to the east), and the axis of the Haditha syncline.



130 The springs and their respective conductivities are from water sampling undertaken by us in 2015, except from the star, which is derived from Khalil (1992). The springs labelled 15A, 15B and 15C are referred to in more detail below. (B) schematic cross-section of sub-surface geology along the black dashed line on the map (X-Y), showing hydrogeological theory predicting the lateral shoreward migration of the interface developed between the hypersaline Dead Sea brine and less saline groundwater ('fresh-saline interface') with time. The two boreholes of El-Isa et al. (1995) are labelled 'BH1' and BH2', as on the map. The vertical exaggeration for the cross section is 40.

### 3 Data and Methods

135 Our data set includes high resolution optical satellite imagery and aerial survey photographs covering the 50-year period from 1967-2017 (**Table 1**). We orthorectified and pansharpened the satellite imagery by using standard algorithms and workflows in the PCI Geomatica software package. For orthorectification of the 2002 – 2010, 2011 – 2013 and 2014 – 2015 satellite imagery, we used the Shuttle Radar Topography Mission (SRTM) Digital Elevation Model (DEM), the Advanced Spaceborne Thermal Emission and Reflection Radiometer (ASTER) DEM, and the Advanced Land Observing Satellite (ALOS) World 3D Digital Surface Model (DSM), respectively. For the Pleiades images from 2016 and 2017, atmospheric  
140 correction, orthorectification and georeferencing were conducted by Airbus against the Astrium Elevation 30 global DEM. All pre-2016 images were georeferenced by using nine Ground Control Points (GCPs). Additional co-registration of pre-2016 imagery was performed with respect to the 2017 Pleiades imagery by using tools from the Geospatial Data Abstraction Library (GDAL) with numerous manually-selected tie-points. In the case of the 1967 image, the use of ESRI online World Imagery was also necessary for  
145 further co-registration due to the geographical limits of the 2017 Pleiades imagery.

Close-range photogrammetric surveys undertaken in October 2014, October 2015 and December 2016 provide yet higher resolution orthophoto mosaics and DSMs (for survey limits, see **Figure 1B**). The surveyed areas were imaged from a helikite or drone at a height of ~100 m with a 16 Megapixel (MP)  
150 Ricoh GR camera (2014), a 12 MP GoPro Hero4 camera with modified lens (2015) or with a 12 MP DJI Phantom 3 inbuilt camera (2016). During each survey, 50-60 temporary GCPs were measured with a Trimble ProXRT differential GPS receiver with real time corrections. Al-Halbouni et al. (2017) detail the procedure for generating these orthophoto mosaics and DSMs. The internal horizontal and vertical uncertainty of the DSMs is estimated to be: 2014 (10 cm, 11 cm), 2015 (12, 17 cm) and 2016 (37, 31 cm).

155



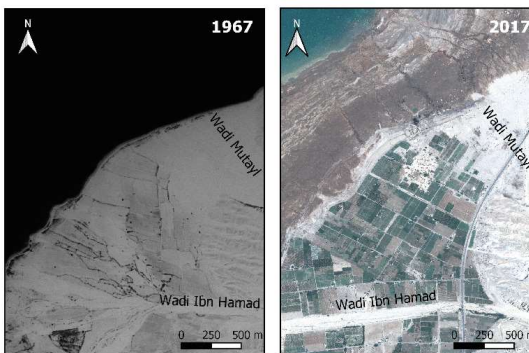
In 2015, we also made a preliminary survey of water sources in the study area. Samples for  $\delta^2\text{H}$  and  $\delta^{18}\text{O}$  were taken unfiltered from springs in bedrock on the landward side of the sinkhole area, from springs within the sinkhole area or on its seaward side, and from ponds within individual sinkholes (**Figure 2A**). Temperature and electrical conductivity were measured in-situ at each sample location with a Hach  
160 HQ40D Portable Multi-meter.  $\delta^2\text{H}$  and  $\delta^{18}\text{O}$  were determined at the UFZ by isotope ratio mass spectrometry (IRMS delta S; Finnigan MAT). For determining  $\delta^{18}\text{O}$  with an analytical precision of  $\pm 0.1\%$ , the standard  $\text{H}_2\text{O}-\text{CO}_2$  equilibration method (Epstein and Mayeda, 1953) was applied.  $\delta^2\text{H}$  was determined using the chromium technique (Gehre et al., 1996), which does not require corrections for salt effects. Analytical precision is  $\pm 0.8\%$ . All isotope ratios are reported relative to the Vienna Standard  
165 Mean Ocean Water (VSMOW).

All data were integrated and analysed within a Geographic Information System (GIS) software package (Q-GIS). The number and extent of remotely-sensed sinkholes represent minima, as local farmers have filled in sinkholes to mitigate disruption to their work. Therefore, we also include information from  
170 sources that undertook earlier field surveys in communication with local farmers (El-Isa et al., 1995; Sawarieh et al., 2000; Closson and Abou-Karaki, 2009). In addition, we combine our mapping of the coastline through time with historical measurements of the Dead Sea level from the Israel Marine Data Center (ISRAMAR) and the Jordanian Ministry of Water and Irrigation (MWI) to reconstruct the former Dead Sea bathymetry in the study area.

175



	Data Source	Aquisition Year(s)	Resolution (m/pix)
Optical Satellites	Corona	1967, 1968, 1970	2.0
	Quickbird	2002, 2004-2007, 2012	0.6
	Ikonos	2006	0.8
	Worldview 1	2008, 2011, 2012	0.5
	GeoEye-1	2009-2010	0.5
	Worldview 3	2014	0.3
	Pleiades 1a	2013, 2015 - 2017	0.5
Aerial Surveys	RJGC Aerial	1981, 1992, 2000	0.6
	Drone and Helikite surveys	2014 - 2016	0.1

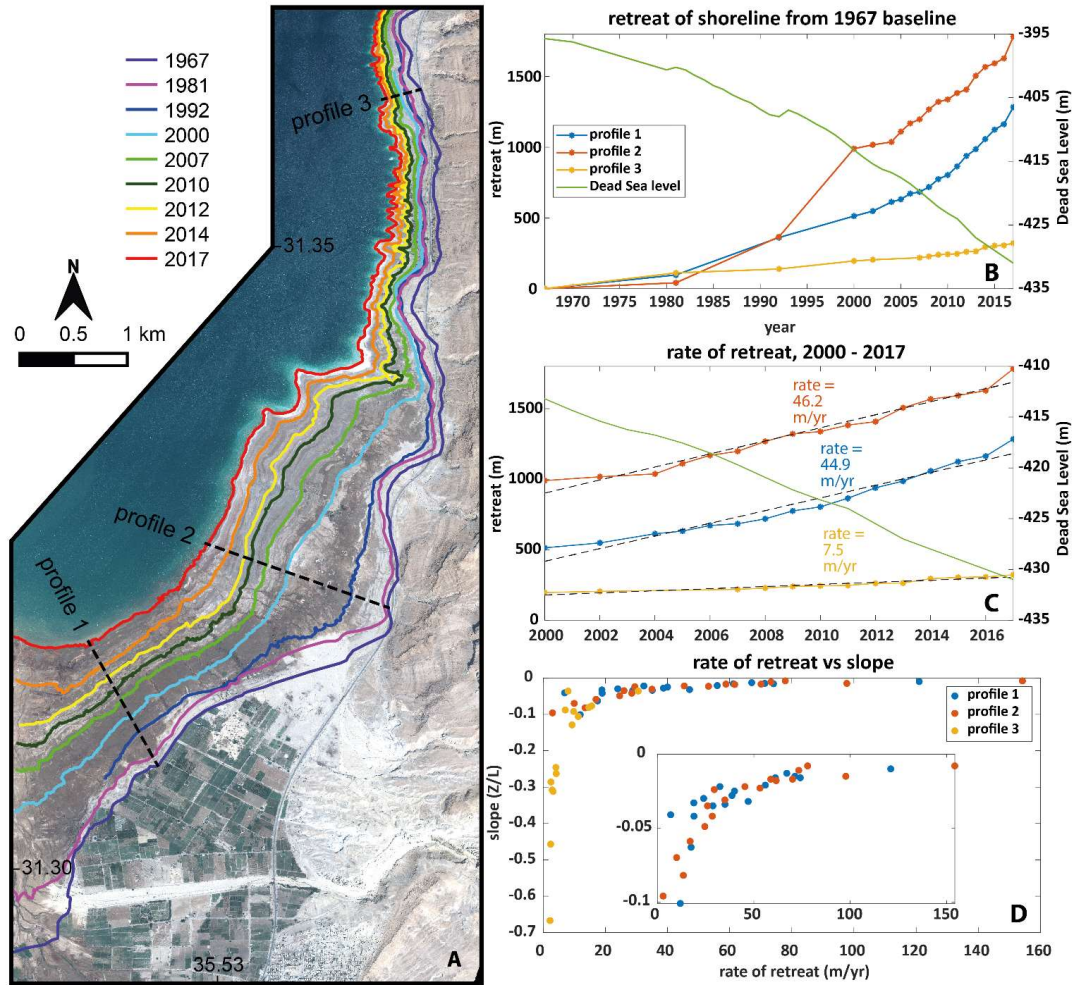


180 **Table 1: Sources and resolution of remote- and near-sensing data used in this study. RJGC = Royal Jordanian Geographic Centre. The spatial resolution of the dataset varies from 1.8 – 0.1 metres per pixel. The temporal resolution of the dataset is decadal from 1970 – 2010, and annual from 2004 – 2017.**

## 4 Results

### 4.1 Base level fall and shoreline retreat

The Dead Sea level drop has resulted in a dramatic retreat of the shoreline in the Ghor al-Haditha area. As of 2017, the shoreline had retreated from its 1967 position by a minimum of 0.3 km in the north to a maximum of 2.5 km in the south. The rate of retreat in the southern part of the study area accelerated from < 10 m/yr between 1967-1980 to an average rate of ~45 m/yr between 2000-2017 (Figures 3 B, C). In the north of the area, the rate of retreat has been a steadier of about 7-8 m/yr. Figure 3D shows that the rate of shoreline retreat is correlated non-linearly with the former bathymetric slope.



190

Figure 3: Dead Sea level fall and shoreline retreat in the Ghor al-Haditha area of Jordan from 1967-2017. (A) Map of shoreline retreat with time, produced from satellite and aerial imagery. Also shown here are plots of the Dead Sea Level and of the shoreline position along profiles in the Ghor al-Haditha area over the periods: (B) 1967-2017 and (C) 2000-2017. (D) Plot of rate of shoreline retreat against bathymetric slope for Profiles 1-3. The inset shows a close-up of the data from Profiles 1-2 for clarity.

195



## 4.2 Surface erosion and deposition

### 4.2.1 Stream channel incision into the former lake bed

Two main stream channel morphologies have been cut into the exposed salty-marl deposits of the former Dead Sea lake bed: meandering (CM) and straight (CS) (**Figure 4**). The heads of all meandering channels have developed at spring points (usually one per channel). Such springs lie either at the alluvium/mudflat boundary or within the mudflat deposits. The heads of straight channels initially developed some distance out on the mudflat, commonly downslope from the terminations of active alluvial fans, and are typically branched.

As the shoreline has retreated, both channel types have grown seaward. While the straight channels also show upstream growth (e.g. CS1-3 in **Figure 4**), most meandering channels show little or no upstream growth (e.g. CM1-4 and CM6 in **Figure 4**). Established sections of both channel types also widen progressively with time. From field observations, channel widening is commonly associated with fault-delimited slumping of the channel sides (Al-Halbouni et al., 2017). These lower sections of the straight channels are commonly braided and contain deposits of sand to cobble clast size. Deposits within the meandering channels are mud to silt size.

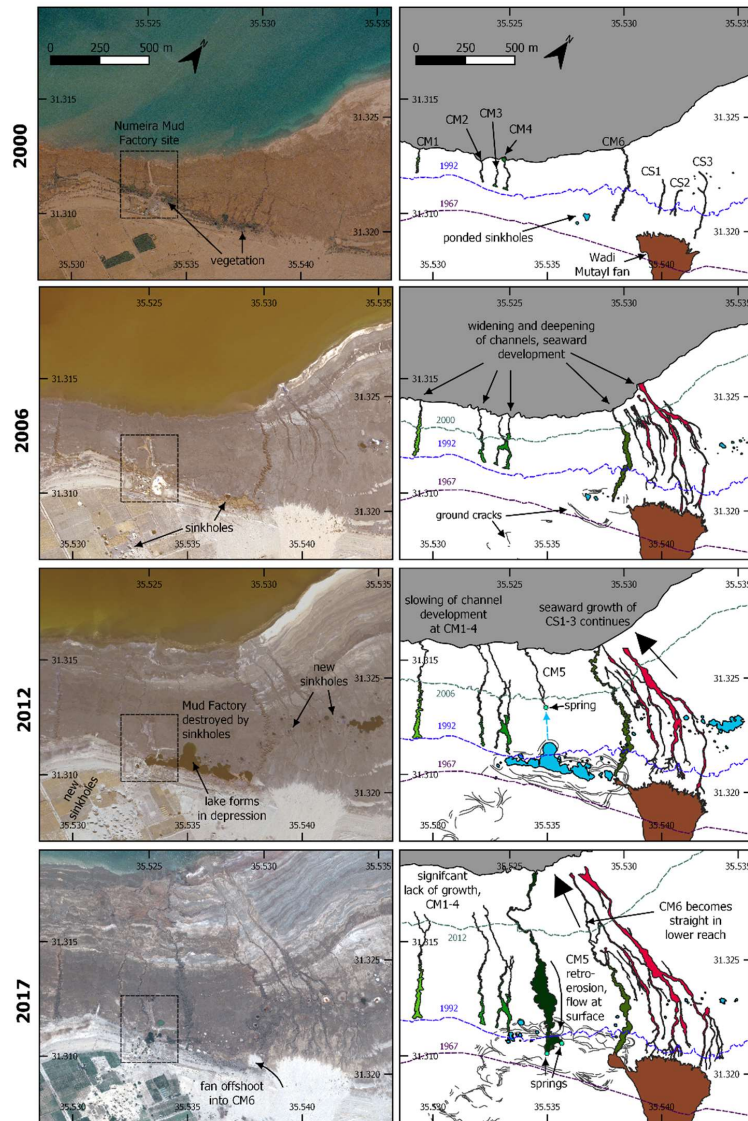
An unusual meandering channel is CM5. This formed in 2012 with its head initially located in the middle of the mudflat (**Figure 4**). Channel incision then progressed rapidly upstream over three months towards the alluvium/mud-flat boundary, in association with the drainage of a lake there (see Al-Halbouni et al., 2017 for details). Co-incident with the establishment of CM5, the growth of nearby meandering channels CM1-4 has diminished markedly.

In profile, both meandering and straight channels are ‘V-shaped’, and they both narrow and shallow seaward along their lengths (**Figure 5**). The straight channels additionally narrow and shallow landward toward the adjacent active alluvial fans. The channel width/depth (W/D) ratio seems independent of the substrate material (salt- or mud-dominated) (**Figure 6A**). All channels in all materials display W/D ratios of 3 – 15 in the channel half nearest the channel head. Straight channels show markedly increased W/D

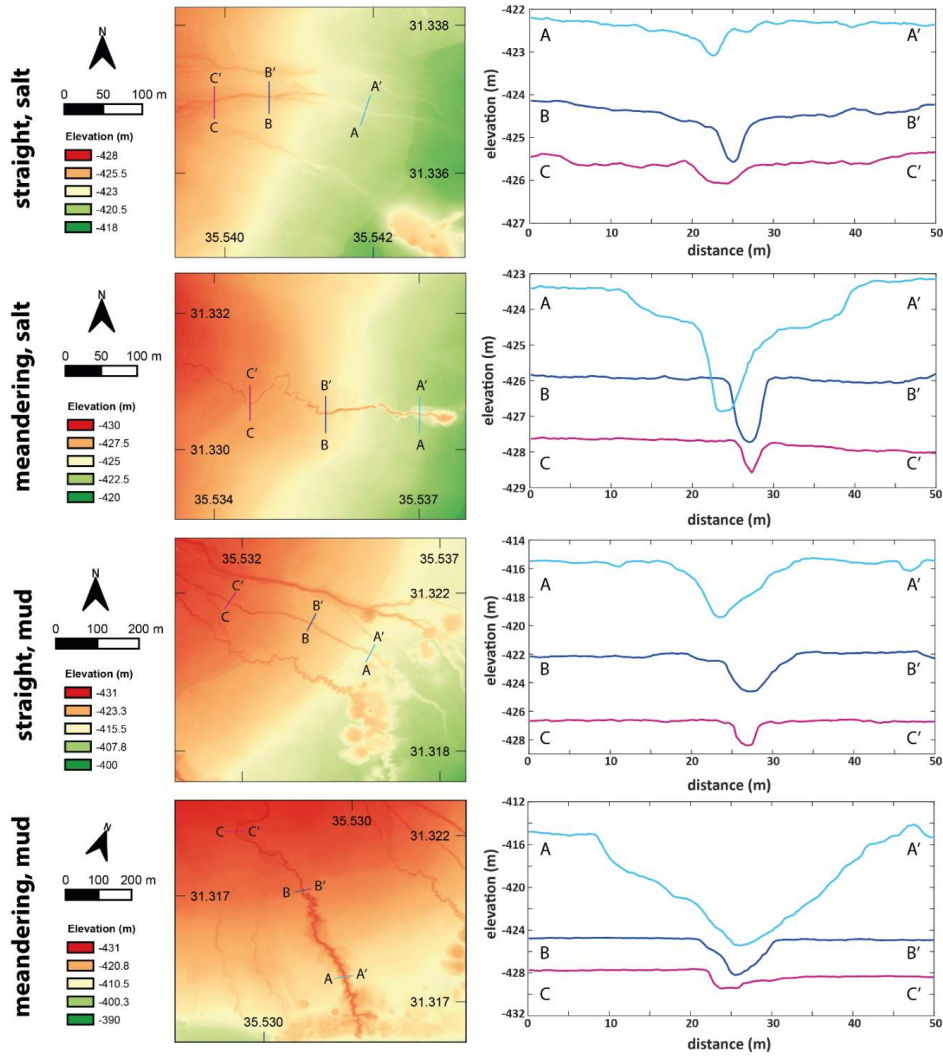


ratios of 10-40 in their lower sections (**Figure 6A**), however, a variation that is associated with decreasing  
225 slope of the former seabed (**Figure 6B**). In contrast, W/D ratios of meandering channels remain  
unchanged as one progresses downstream, and are apparently unrelated to slope. Sinuosity of the  
meandering channels is 1.1-1.7, with a general slight increase along the upper three quarters of the  
channels, then decreasing to 1.1-1.3 in the lowermost reach (**Figure 6C**). Development of sinuosity in the  
meandering channels also seems independent of slope (**Figure 6D**).

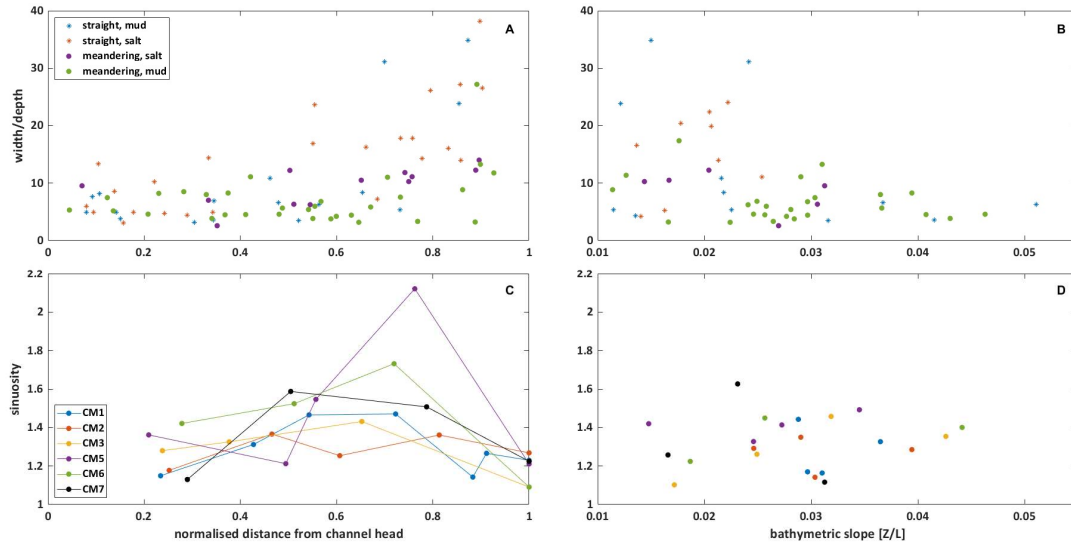
230



235 **Figure 4:** Evolution of meandering and straight/braided stream channels in the salty mudflat deposits from 2000–2017. The left column shows aerial or satellite imagery. The right column shows maps of channels (red = straight/braided, green = meandering), the Wadi Mutayl alluvial fan (brown), ground cracks denoting the limits of a large-scale depression, and depression or sinkhole-hosted ponds (blue). Dashed purple, blue and green lines indicate the 1967, 1992 and 2006/2012 shorelines, as labelled.



240 **Figure 5: Representative cross-sectional profiles of stream channels incised into the exposed lacustrine deposits of the former lake bed. Left column shows the 2016 photogrammetric DSM with profile locations; Right column shows the channel profiles.**



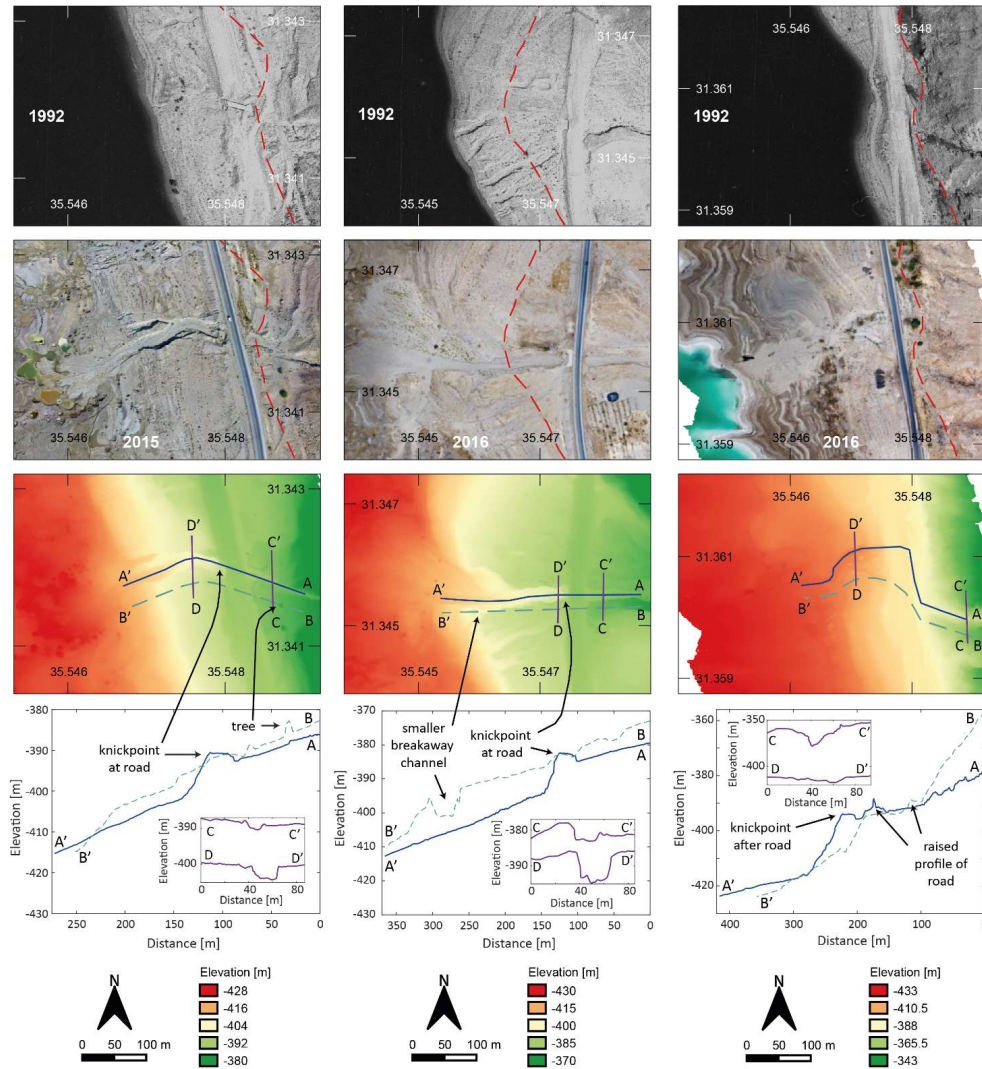
245

**Figure 6: Quantitative analysis of channel geomorphology. (A) Plot of W/D ratio along the lengths of representative meandering and straight stream channels (locations in figure 1). (B) Plot of W/D ratio against former bathymetric slope. (C) Plot of sinuosity along meandering channels (locations in figure 1). Distance is from head to mouth following the maximum valley slope. (D) Plot of sinuosity against former bathymetric slope.**

#### 4.2.2 Stream channel incision into the old marginal alluvial fans

250

Stream channel incision has also occurred into the pre-recession alluvial fan deposits at the former Dead Sea margin (**Figure 7**). Data here are presented for channels related to the new alluvial fans 2 - 4, as they are covered by our close-range photogrammetry surveys, but similar incision is seen in the larger Wadi Mutayl fan also. These channels have W/D ratios of 2 - 6 and, in contrast to the channels in the exposed lake bed, are trapezoid-shaped in cross sectional profile. Deposits within the channel are of coarse sand, gravel and cobbles.



255

260

**Figure 7: Alluvial channel incision and fan growth proximal to the Dead Sea highway [Jordan Valley Highway 65]. Top row: aerial imagery from 1992, taken during the road construction. The dashed red line is the 1967 shoreline. Second row: orthophotos from the 2015 (fan 2) and 2016 (fan 3, fan 4) photogrammetric surveys. The channels incise into the old alluvial fan deposits, with fresh deposition of fan material onto the old lake bed. Older alluvial fan deposits appear darker grey in the orthophoto, whereas fresh deposits are lighter coloured. Third row: DSMs derived from respective photogrammetric surveys. Bottom row: topographic profiles along the channels (A-A') and along the non-incised fan adjacent the channel (B-B'). Also shown are profiles immediately upstream (C-C') and downstream (D-D') of the road bridges.**



### 4.2.3 Alluvial fan growth

In addition to fluvial erosion, fluvial deposition has caused alluvial fans to prograde onto the former Dead  
265 Sea bed from adjacent wadis (**Figures 4 and 7**). The absolute growth of these fans in terms of area varies  
over several orders of magnitude (**Figure 8A**) depending on wadi size. Fan growth at the mouth of the  
Wadi Ibn Hammad has curtailed by engineering works in the 1980s to restrain and straighten its course  
down to the shoreline (See **Table 1**). Normalised growth rates from 2002 onward are generally higher in  
270 the northern part of the area (**Figure 8B**). This perhaps reflects the belated uncovering of the salt- or mud-  
flat there.

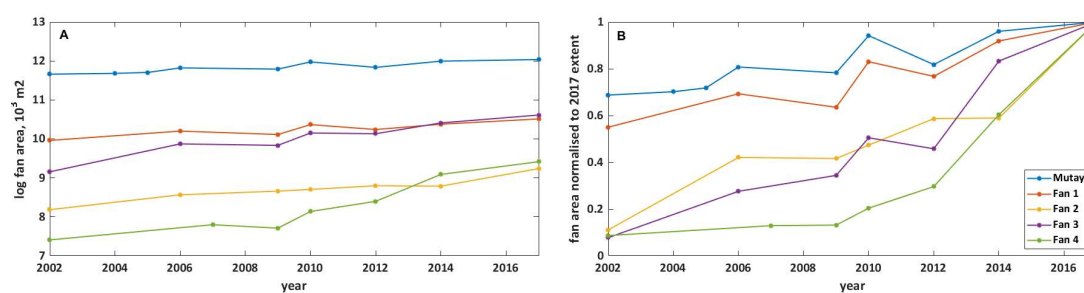


Figure 8: Alluvial fan growth in the study area from 2002 to 2017, in terms of (A) absolute areas and (B) area normalised to 2017 values. For fan locations, see Figure 1.

275



### 4.3 Surface subsidence and collapse

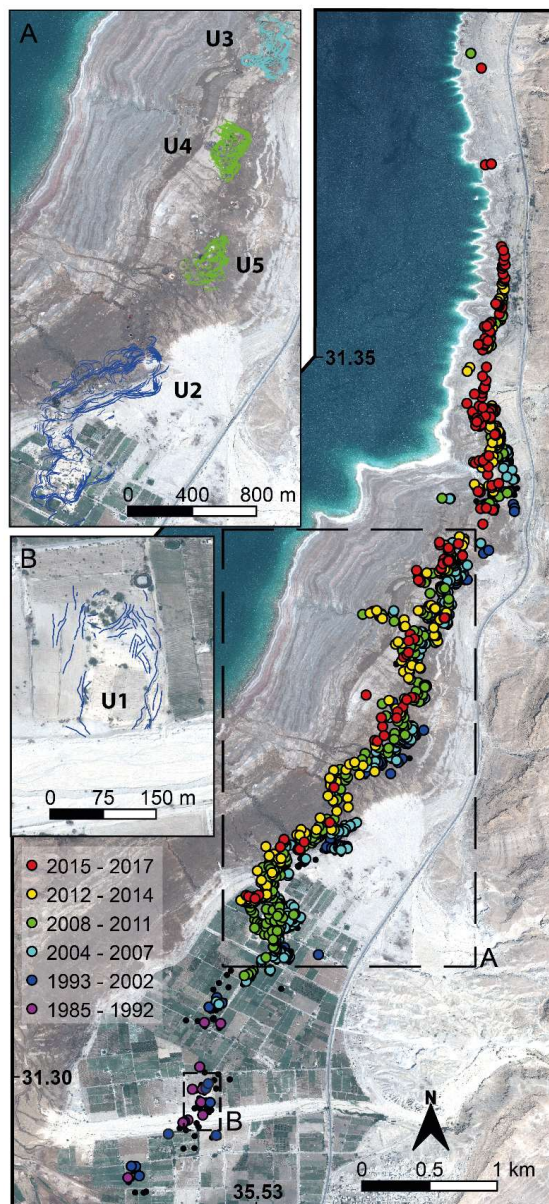
#### 4.3.1 Sinkholes

Sinkhole formation began at Ghor al-Haditha in the mid-1980s in the southern part of the study area  
280 **(Figure 9)**. Initiation of new sinkhole development subsequently shifted north-northeast-ward, roughly  
parallel to the coastline. The most active area is now adjacent the Dead Sea highway in the northern part  
of the study area. In detail the sinkholes have initiated in clusters, with gaps between earlier clusters filled  
or reduced as new sinkholes and sinkhole clusters form. After initiation, sinkhole development has  
generally migrated seaward to variable extents of between 100 – 500 m.

285

The growth rate of the sinkhole population at Ghor al-Haditha was exponential between 1985 and 2009,  
but it has been roughly linear from 2009-2017 **(Figure 10)**. With a notable peak in 2005 also, the  
maximum occurred in 2009 with 134 new holes. Since 2009, the rate of sinkhole population growth has  
stabilised at ~60 new holes per year. We estimate that at least ~1150 sinkholes have formed in the area  
290 between 1985 and 2017.

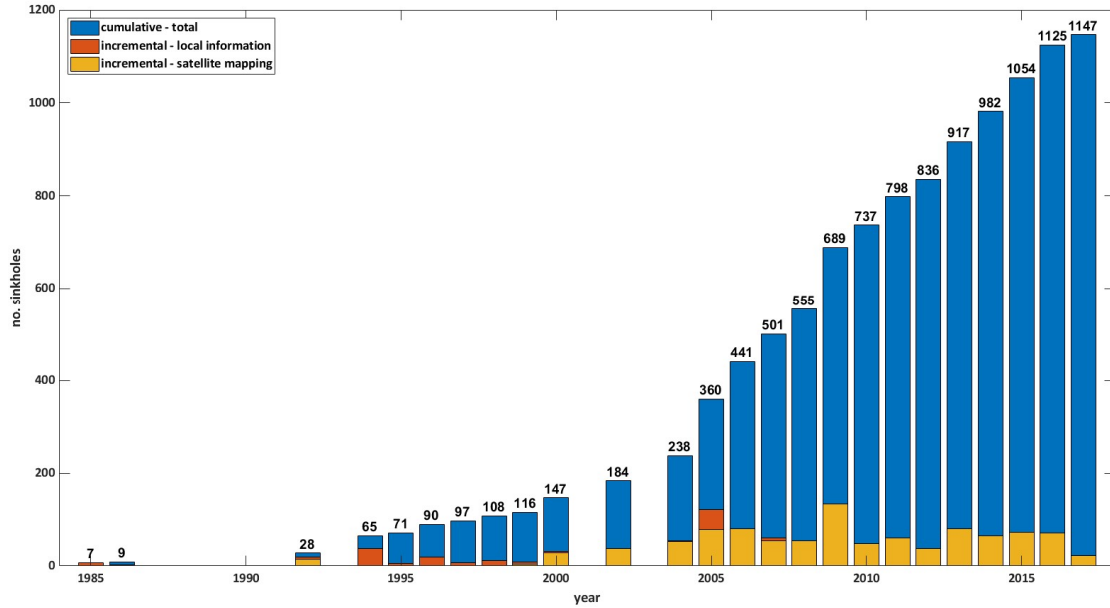
The size and morphology of individual sinkholes is linked loosely to the material in which they form  
**(Figure 11)**. In general, sinkholes have diameters of 1 - 40 m, but some sinkholes in the mud-dominated  
lacustrine deposits have diameters of over 70 m **(Figure 11A)**. The mode of sinkhole diameter is 4 – 8 m  
295 in ‘salt’, 4 – 12 m in alluvial sediments, and 8 – 16 m in lacustrine ‘mud’. Holes formed in the mud- and  
salt-dominated materials have lower depth/diameter ( $D_e/D_i$ ) ratios than holes formed in alluvial  
sediments **(Figure 11B)**. Alluvium-hosted holes show the least variance from the linear regression model  
calculated; mud-hosted holes are highly variable in their  $D_e/D_i$  properties. Regardless of materials,  
eccentricity of sinkhole circumferences is usually 1 – 2; values greater than 2 are rare **(Figure 11C)**.





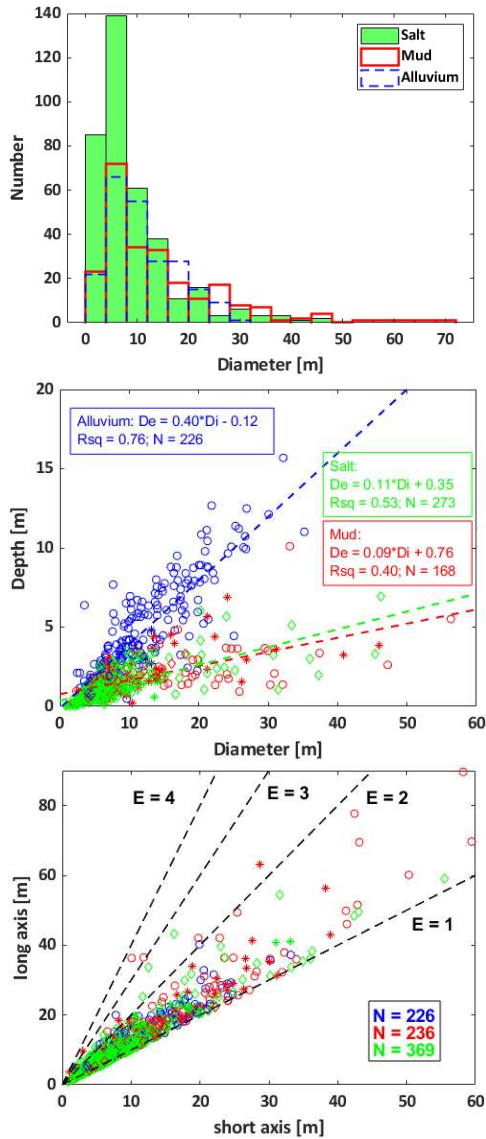
305

Figure 9: Sinkholes mapped from satellite and aerial imagery, colour-coded by year of first sighting in time intervals as labelled. Base image is Pleiades 2017. Smaller black dots are sinkholes mapped prior to 2009 by other sources but not visible in our imagery. Insets A and B show the larger-scale depressions, as denoted by mapped ground cracks and fractures. For clarity, all fractures for each depression are colour-coded by year of first sighting of any fractures related to that depression. In detail, the fracture formation ages in each large-scale depression span a greater range than shown here (see Figures 12 and 13).



310

Figure 10: sinkhole population growth with time in the study area. ‘Local information’ constitutes sinkholes noted in field surveys along with information provided by farmers on sinkholes that were filled in before they were mapped. The total number of sinkholes mapped from satellite imagery alone is 996. The year 2017 appears to have a reduced number of new holes: this is a sampling artefact as there is only a four-month time interval between the 2016 orthophoto and the 2017 satellite image.



315

Figure 11: Morphological characteristics of the sinkhole population developed at Ghor al-Haditha in various sedimentary materials. (A) Number of holes binned according to average diameter, (B) the relationship between depth and diameter, and (C) plan-view eccentricity (longest/shortest diameter). The total number of holes analysed is 226 in the alluvium, 236 in the mud-dominated



320 lacustrine deposits ('mud') and 369 in the salt-dominated deposits ('salt'). Water-filled holes were excluded from the depth/diameter  
analysis. The De/Di plot presents the maximum elevation difference between the rim and the bottom of each sinkhole.

#### 4.3.2 Uvalas

Many sinkholes in the study area have developed within *uvalas* - gentle depressions of several hundred  
325 metres in lateral extent ( $De/Di$  ratios = 0.015 – 0.033) (**Figures 9, 12 & 13**). The uvalas are bounded  
partly by systems of ground cracks and/or by faults with vertical displacements of up to 1.5 m. The  
expression of such fractures is material dependent. Subsidence-related displacements are accommodated  
on fewer but larger fractures in alluvium, whereas numerous but smaller fractures occur in mud-rich  
deposits. As shown below, these fractures are spatially and temporally associated with subsidence of each  
330 uvala. They are not to be confused with regional tectonic structures.

Development of each uvala follows precursory sinkhole formation at that site. 2 – 8 years after the first  
sinkhole sighting (in which time many sinkholes have generally clustered about the initial hole), ground  
cracks develop that no longer trend concentrically to any single sinkhole, but instead delineate a wider  
335 zone of subsidence that envelopes several sinkholes or even several clusters of sinkholes. The first uvala,  
U1, developed between 1992 and 1999 in the south of the area, near the Wadi Ibn Hamad (**Figure 9**). U2  
and U3 initiated in 2002 and 2005-2006, respectively, to the north east of U1. Both U4 and U5 began  
forming around 2008, but lie between U2 and U3. Groundcrack patterns observed in the 2015 and 2016  
orthophotos between Fans 1 and 2 suggest that a new uvala may develop further northeast of U3. In  
340 general therefore, younger uvalas have formed to the northeast, as seen for the sinkholes, although not  
(yet) in as clear a sequence.

After initiation, uvala growth is closely linked with further sinkhole formation within it. For instance,  
groundcracks related to U2 initiated around two spatially-discrete sinkhole clusters; these fractures sets  
345 propagated and joined as sinkhole development migrated (**Figure 12**). For both U3 and U4, two 'prongs'  
of coeval crack and sinkhole development are visible (**Figures 12 and 13**). Conversely, U1 ceased  
development by 2006, in tandem with diminished sinkhole activity nearby. Similar to the sinkhole



population growth trends, the expansions of the uvalas U2, U3 and U4 has been mostly seaward and accelerated markedly in 2008-2009 (Figure 14).

350

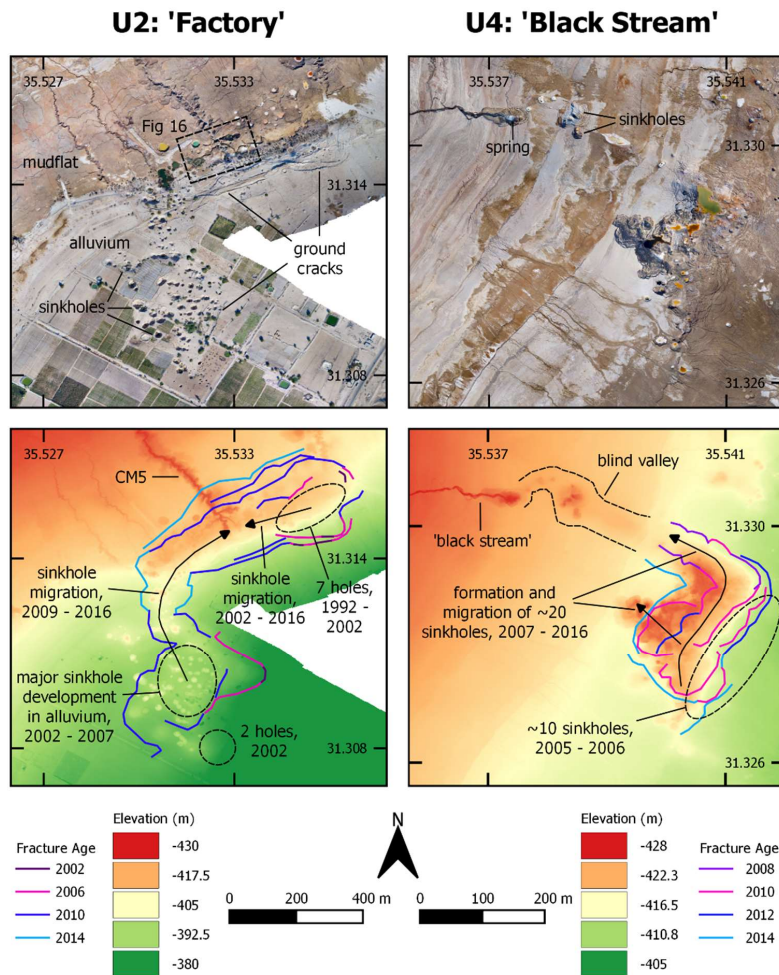


Figure 12: Structural development of uvalas with demonstrable connection to channelized subsurface water flow. See figure 9 for locations. The years of formation of the main depression-bounding fractures (i.e. when first visible in imagery) are grouped and coloured in four-year intervals for U2 and in two-year intervals for U4. Each uvala is linked morphologically to a highly active stream that emerges on the seaward side at several meters below the surrounding ground surface.

355

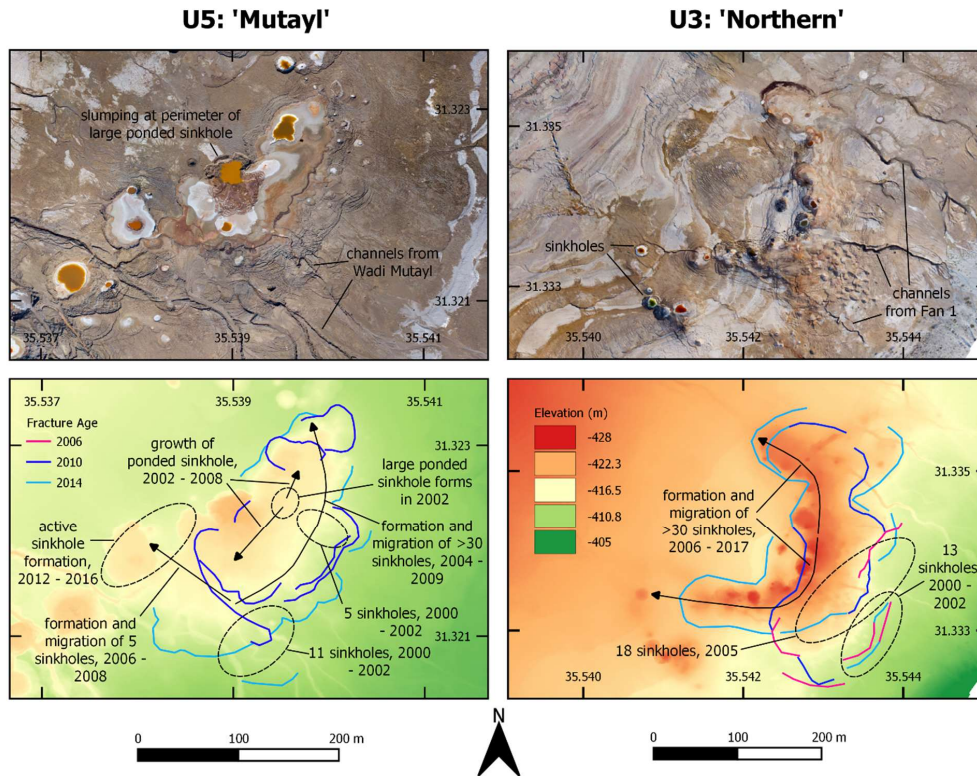


Figure 13: Structural development of uvalas U5 and U3 with unclear connection to subsurface water flow. The years of formation of the main depression-bounding fractures (i.e. when first visible in imagery) are coloured in four-year intervals.

360

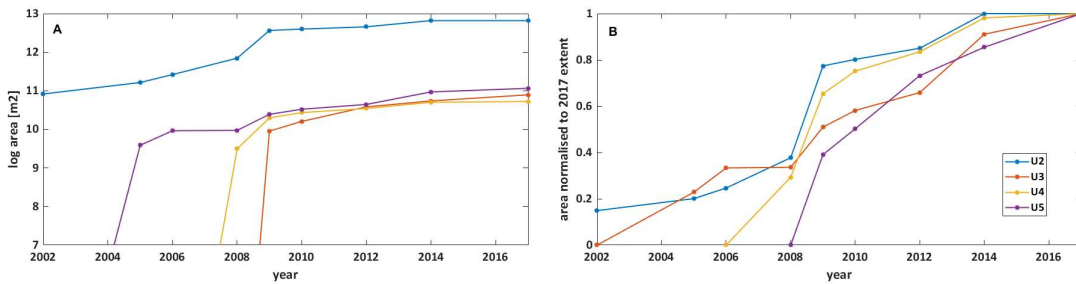


Figure 14: Growth of uvalas in the study area, shown as (A) absolute areas and their (B) area normalised to that in 2017.



#### 4.4 Notes on properties of surface water and groundwater

##### 4.4.1 Springs and streams

365 Springs within the Ghor al-Haditha sinkhole area can be categorised as sulphurous or non-sulphurous  
(**Figure 2A**). The water temperatures of both spring types were between 27.7-30.6 °C. Non-sulphurous  
springs emerge from the Ajlun Group aquifer (**Figure 15A**) and from near the alluvial/lacustrine sediment  
boundary in the south of the area (**Figure 15B**). Sulphurous springs are most common in the north of the  
area, where they emerge from the salt-rich deposits, and are characterised by dark, turbid water, with gas  
370 bubbles and a strong smell of H<sub>2</sub>S (**Figure 15B**). Sediments surrounding such springs commonly show a  
black, green or reddish staining. Sulphurous springs have also been recorded historically in the adjacent  
outcrops of the Ram-Kurnub aquifer (**Figure 2A**) (Khalil, 1992).

Electrical conductivity values of the spring waters show an extremely wide range (1-217 mS), but a well-  
375 defined spatial distribution (**Figure 15D**). Conductivity values of springs emerging from Ajlun Group  
bedrock are 1-14 mS, while values of 13-78 mS characterise streams emerging in the mud-rich sediments  
on the seaward side of the sinkhole-affected area (**Figure 2A**). The highest conductivity values – some  
higher than the value of the Dead Sea itself (180 mS) - were measured for sulphurous springs emerging  
in the salt-rich sediments in the north of the area (**Figure 2A**). The δ<sup>2</sup>H and δ<sup>18</sup>O composition of all  
380 spring waters plot below the local recharge values, which are marked by the Eastern Mediterranean  
Meteoric Water Line (EMMWL) (**Figure 15E**). Fresh to brackish groundwaters from the Ajlun Group  
and the superficial alluvium aquifer are isotopically lightest, referring to regional recharge that  
experienced slight evaporation before infiltration. Sulphurous springs are isotopically heavier, possibly  
due to admixture of highly enriched interstitial brines hosted within the salt-flat sediments (cf. Siebert et  
385 al., 2014).

Discharge rates of the largest active streams were estimated near their source springs during the 2015  
field campaign. These included the main stream in CM5 (discharge = 0.20 m<sup>3</sup>/s) near the destroyed factory  
site, the ‘black stream’ in CM7 (discharge = 0.07 m<sup>3</sup>/s) emerging in the centre of the area and the stream

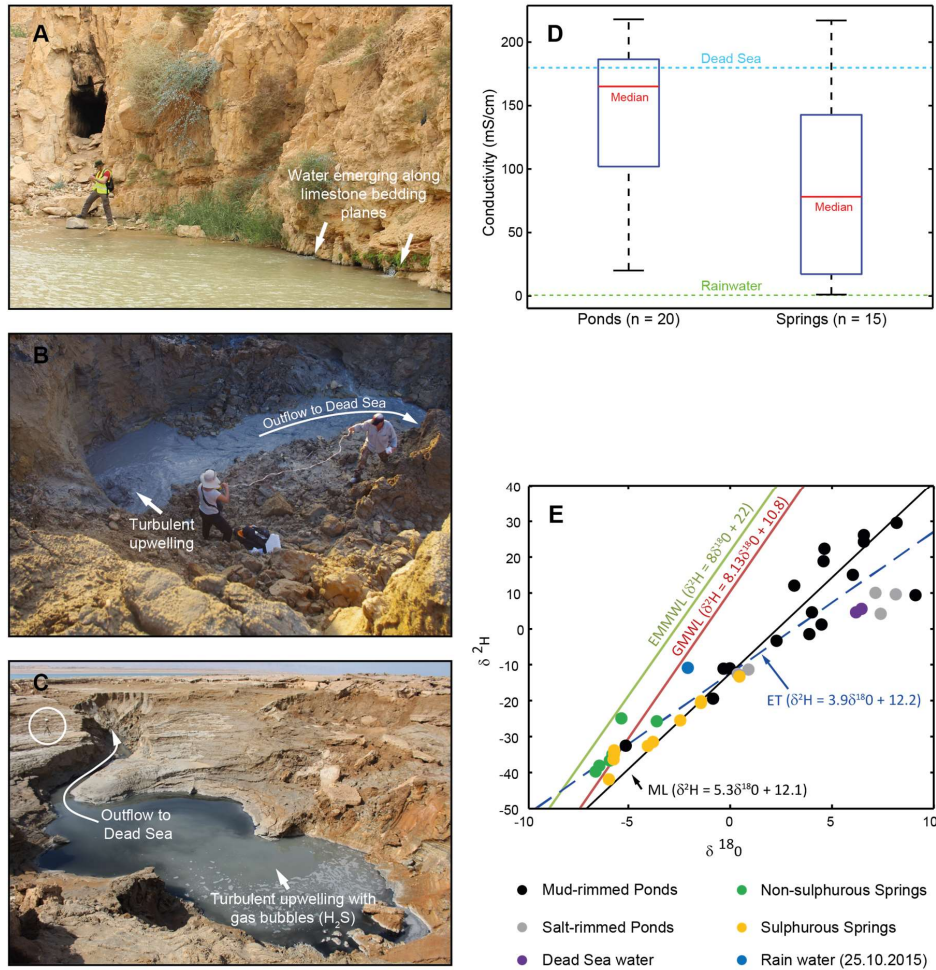


390 in CM8 (discharge = 0.04 m<sup>3</sup>/s) in the north of the study area. Most of the other channels in the area were  
of much lower discharge or had no discharge during field campaigns in 2014-2016.

#### 4.4.2 Ponds

Ponds within sinkholes range markedly in water colour, organic content (algal/bacterial scum) and salt  
rim development. The electrical conductivity of ponds (47-218 mS) is generally higher than the springs  
395 (**Figure 15D**). Highest values were recorded for ponds in salt-rich sediments, but values varied greatly  
even between adjacent ponds of similar appearance (**Figure 2A**). Pond water temperatures ranged from  
26.0-32.4 °C.  $\delta^2\text{H}$  and  $\delta^{18}\text{O}$  signatures in pond brines are heaviest among all observed fluids, mainly due  
to strong admixture of interstitial brines and due to high evaporation within ponds. Brines in mud-edged  
ponds represent the isotopic heaviest fluids in a mixing line (ML in **Figure 15E**) between fresh/brackish  
400 groundwaters (green in **Figure 15E**) and interstitial brines. However, isotopic signatures in brines stored  
in salt-edged ponds deviate from that mixing line due to much higher evaporation, leading to higher  
salinity and subsequent precipitation of the observable salts. The overall trend is consistent with effect of  
evaporative fractionation, and the line (ET in **Figure 15E**) that best fits the data ( $R^2 = 0.9$ ) has a slope of  
3.9, which is consistent with such fractionation under arid conditions (relative humidity < 25%).

405



410 **Figure 15: Springs types and electrical conductivity measurements in the Ghor al-Haditha area. (A) Non-sulphurous Al-Maghara**  
 ('the cave') spring in the Wadi Ibn Hamad. White arrows point to water flowing from bedding planes in the limestone of the Aijun  
 bedrock aquifer. Person for scale. View is to the east. (B) Non-sulphurous spring formed between Oct. 2014 and Oct. 2015 at the  
 415 head of channel CM5 (see also Figures 1 and 4) in the mud-rich lacustrine deposits. Grey-lilac colour is from suspended mud load.  
 The spring lies about 5 m below the top of the lacustrine deposits, from where the image was taken. (C) Sulphurous spring at the  
 head of Channel CM6 ('Black stream') in salt-rich lacustrine deposits. A 35 cm high GPS tripod is circled for scale. The spring lies  
 about 2-3 m below the former lake bed. The water colour is cloudy, dark-grey or blackish. The froth at the surface is from gas (H<sub>2</sub>S)  
 bubbles. (D) Electrical conductivity of ponds (water-containing sinkholes) and springs in the Ghor al-Haditha area. Also shown for  
 reference are the conductivities of local rainwater and the Dead Sea water. (E)  $\delta^2\text{H}$  and  $\delta^{18}\text{O}$  data for springs and water-containing  
 sinkholes in the Ghor al-Haditha area. Eastern Mediterranean Meteoric Water Line (EMMWL) from Gat and Dansgaard (1972)  
 and Global Meteoric Water Line (GMWL) taken from Dansgaard (1964). Mixing Line (ML) and evaporation trend (ET) line.



## 5 Discussion

### 5.1 Base-level fall and shoreline retreat

420 Our results as presented above clearly demonstrate that the evolution of various geomorphological phenomena in the Ghor al-Haditha area, which include new fluvial channels and alluvial fans, as well as new sinkholes and uvalas, are intrinsically linked to a common driver: the fall in regional hydrological base level resulting from the drying of the Dead Sea. In particular, the base level fall has exposed a large area of the former Dead Sea bed to fluvial erosion and deposition as a consequence of shoreline retreat.

425 The spatiotemporal variation in the rates of retreat result from the temporal variation in the rate of base-level fall and, more importantly, the spatial variation in the local bathymetry (**Figure 3**). The northern part of the study area had a steeper bathymetry, reflecting its proximity to the bounding fault scarp of the Dead Sea basin (**Figure 2A**). The southern part of the area had a gentler bathymetry, possibly reflecting the extensive Plio-Pleistocene and Holocene fan deposition at the terminations of several major wadis

430 (**Figure 1C**). This variation in bathymetry and rate of shoreline retreat represents the framework for the past and the future geomorphological changes.

### 5.2 Geomorphic characteristics of new stream channels in cohesive lacustrine materials

At Ghor al-Haditha, channels that formed display distinct map-view morphologies: meandering and straight/braided. Such differences in morphology result from a complexly interacting set of factors,

435 including (i) the flow discharge, (ii) the slope prior to channel formation (iii) the sediment load characteristic and (iv) the properties of the material into which the channel is cut (Buffington and Montgomery, 2013; Leopold and Wolman, 1957; Schumm and Khan, 1972). Since the Ghor al-Haditha channels have formed in the same cohesive lacustrine sediments and along similar bathymetric profiles, we deduce that the observed differences in map-view morphology arise from differences in discharge rate

440 and sediment load. Specifically, we infer that the meandering channel geometries stem from steady, low discharge of groundwater from springs and a silty clay sediment load. In contrast, we infer that the straight channels are fed by episodic higher-discharge events (flash floods) from nearby wadis bearing higher volume and coarser sediment loads. Such inferences are supported by our field observations of sediment deposits within each channel type.



445 In cross-section, the two channel types show v-shaped profiles with average W/D ratios of 5 - 15 (**Figures**  
**5 & 6**). Such W/D ratios are thought to be typical of single thread or anastomosed channels in cohesive  
materials (Church, 2006; Simon and Darby, 1997), although field studies of channels in such materials  
are rare (Vachtman and Laronne, 2013). Similar but more tightly constrained W/D ratios of 12-15 are  
450 reported for rivers with clay-dominant substrates by Ebisa Fola and Rennie (2010). The straight channels  
(CS1-6) show some higher W/D ratios (20 – 40) in their downstream sections close to the shore, however.  
These channel sections correspond to areas of lowest slope (**Figure 6B**), and so could be influenced by  
that factor. Another factor, possibly complementary, is that landward growth toward the alluvial fan  
(**Figure 4**) had facilitated greater discharges and sediment loads by the time these lower sections formed.

### 5.3 Geomorphic characteristics of new stream channels in non-cohesive alluvium

455 In contrast to the v-shaped channel cross-sections in the mudflats, trapezoidal cross sections observed in  
the marginal alluvium (**Figure 7**), which match well with observations on the western shore of the Dead  
Sea (Bowman et al., 2010). The cross-section profiles and the straight/braided map-view geometry of  
these channels are consistent with controls of relatively high discharge vs slope (Leopold and Wolman,  
1957), and of low substrate cohesion (Schumm and Khan, 1972; Peakall et al., 2007).

460

Channel incision into the old marginal alluvium represents a hazard to infrastructure - specifically the  
adjacent north-south highway along the Dead Sea's eastern shore (**Figure 7**). Constructed in the early  
1990's, the road section lies close to, and in places seaward of, the 1967 shoreline. Reinforced concrete  
bridges and drains were emplaced at intersections with wadis to guide stream water under the road. The  
465 foundations of some of these bridges now lie at knickpoints in the stream profiles, with enhanced erosion  
at their downstream sides. The future development of such erosion and bridge integrity should be  
monitored closely.



#### 5.4 Effect of base level fall on channel morphology in space and time

470 The most obvious effect of base level fall on the channel development at Ghor al-Haditha is the  
progressive seaward incision of newer channel segments into the lacustrine deposits as the shoreline  
retreats over time (**Figure 4**). Coeval with incision of new channel sections, we also observe progressive  
widening of existing upstream sections. For the meandering channels, the relatively constant W/D ratios  
475 along the present channel profiles (**Figure 6A**) show that these older channel sections must have also  
deepened with time. Finally, the gradual decrease in sinuosity seen for older channel sections (**Figure  
6C**), which is independent of slope (**Figure 6D**), suggests that sinuosity has also progressively decreased  
with time. The persistence of such changes in time and space in such small scale channels suggests that  
the continuous base level fall has inhibited the development of equilibrium channel geometries (cf. Simon  
and Darby, 1997).

480

The pattern of sinuosity variation along the channel length (**Figure 6C**) is compatible to some degree  
with conceptual model predictions for effects of incremental base level fall. Schumm (1993) proposed an  
increase in sinuosity only in the lowermost channel sections for an increment of base level fall. This  
concept is agreement with the observed sharp increase in sinuosity immediately up stream of the channel  
485 mouths (**Figure 6C**). Subsequent continuous base level fall may account for the observed gradual  
decrease in sinuosity further upstream, as (1) the lowermost channel section progressively migrates  
seaward and (2) overall channel slope increases (Yoxall, 1969).

Head-ward adjustment differs for each channel type, however. The heads of straight channels migrate  
490 landward (upslope); the heads of meandering channels deepen rather than migrate. The upslope incision  
and migration of the channel head in the straight channels is consistent with experiment results from Koss  
et al. (1994), in which base level fall occurred across a substrate with a marked change of gradient. As  
base level in the experiment fell, the channels developed at a transition from gentle to steeper slope and  
then progressively deepened and eroded headward. A similar variation in slope geometry is present  
495 between the Wadi Mutayl fan and the area where heads of straight channel CS1-3 initially formed  
(compare **Figures 3 and 4**). In contrast, the heads of most meandering channels are fixed in space and



time (**Figure 4**), simply because the power of subsurface flow (a function of slope and discharge) inland of the spring points is insufficient to destabilise the overburden there. An exception to this behaviour is seen in channel CM5 (**Figures 4 and 16**), which has the highest measured discharge of all the meandering channels.

500

### 5.5 Sinkhole morphology and spatial distribution

The contrast in morphology of sinkholes formed in alluvium or mud-rich lacustrine materials at Ghor al-Haditha (**Figure 11A, B**) is also observed elsewhere around the Dead Sea (Filin et al., 2011; Al-Halbouni et al., 2017). The lower  $D_e/D_i$  ratios of the mud-hosted sinkholes and their longer tail in size distribution toward diameters greater than 70 m has been attributed to contrast in strength (Al-Halbouni et al., 2018) and/or rheology (Shalev and Lyakhovskiy, 2012) of these materials. The high strength and/or frictional rheology of the alluvium inhibits lateral expansion of the sinkhole as it deepens, whereas the low strength and/or viscoelastic rheology of the mud-rich sediments enables lateral expansion while reducing the depth.

510

Expanding upon data presented by previous authors (cf. Filin et al., 2011; Al-Halbouni et al., 2017), we show that  $D_e/D_i$  ratios of sinkholes formed in salt-rich lacustrine sediments generally fall between those of sinkholes formed in alluvium or mud-rich lacustrine sediments (**Figure 11B**). Compared to those in mud-rich sediments or alluvium, sinkholes formed in the salt-rich sediments also have generally smaller diameters (**Figure 11A**). This could reflect a scaling limit imposed by the level of karstification, which in the salt-rich material in the northern part of the area is at, or within a few metres of, the surface.

515

At the kilometre scale, the spatial distribution of sinkholes at Ghor al-Haditha follows two linear trends: a  $N24^\circ$  trend in the south and a  $N10^\circ$  in the north (**Figure 9**). These trends match those of main regional faults in the Dead Sea transform (**Figure 1A**) and so indicate a tectonic control on overall sinkhole distribution (cf. Closson and Abou Karaki, 2009). Similar tectonic controls have been suggested on the spatial distribution of sinkholes on the Dead Sea's western shore (Abelson et al., 2003; Yechieli et al., 2016). In closer detail (hundred-metre scale), the sinkhole distribution is non-linear or sinuous (**Figure**

520



9). This non-linearity may reflect control from the distribution of salt-rich deposits at depth (Ezersky et al., 2013), and thus reflect the palaeo-shoreline, as determined by the regional fault systems.

## 5.6 Uvalas

The uvalas at Ghor al-Haditha (**Figures 9, 12 and 13**) are distinct from the sinkholes in terms of their scale and morphology. The uvalas are much more irregular in plan-view and have  $D_e/D_i$  ratios an order of magnitude lower. Their irregular shape indicates material removal in a ‘linear’ or ‘areal’ sense as opposed to shape being governed by material removal at a point, as is the case with sinkholes.

The exact definition of uvalas and the processes contributing to their formation are still debated in karst geomorphology (Ćalić, 2011; Kranjc, 2013; Lowe and Waltham, 1995). The shallow but laterally extensive morphologies of the salt-karst uvalas at Ghor al-Haditha agree well with Ćalić (2011)’s observations of uvalas in shallow limestone karst where the water table is close to the base of the depression, which causes the characteristic ‘widening without deepening’ evolutionary pattern. Uvalas are distinct from *poljes* (the second most diagnostic karstic depression after *dolines*, sometimes considered to be the karstic equivalent to a fluvial valley) in that their bottom is always situated above the karst water table and is generally more undulating and often pitted with sinkholes (Ćalić, 2011).

540

Our observations at Ghor al-Haditha provide new insight into the development of salt-karst uvalas. There is a clear spatiotemporal link between initial sinkhole clusters and the uvala formation (**Figures 9, 12 and 13**). In all cases, some precursory sinkhole development occurred several years before. The development of the uvalas after this precursory sinkhole formation is linked with further sinkhole formation. Uvala formation and sinkhole development initiate develop and cease in tandem, thus indicating the same overall formation process.

545

## 5.7 Effects of base-level fall on sinkhole development

A striking observation from our study is that, similar to the fluvial channels, sinkhole clusters consistently show a seaward growth after they have been established (**Figure 9**). Several past studies on the Dead Sea



550 sinkhole problem have postulated that the fall of base level should affect the interface developed between  
the hypersaline Dead Sea brine and less saline, brackish (i.e. relatively ‘fresh’) groundwater (Salameh  
and El-Naser, 2000; Yechieli, 2000; Yechieli et al., 2009) (**Figure 2B**). In theory, this ‘fresh-saline  
interface’ should shift seaward in tandem with the retreating shoreline, enabling groundwater  
undersaturated with respect to halite to infiltrate the salt-rich deposits in the subsurface, thus triggering  
555 karstification and surface subsidence. A prediction of this theory is that karstification and new sinkhole  
development should shift seaward also, although evidence on the western shore for such shift is weak  
(Abelson et al., 2017; Charrach, 2018). Although we lack constraints on the fresh-saline interface from  
sources boreholes or geophysical techniques in the Ghor al-Haditha study area, our observations of  
systematic shoreward sinkhole migration provide the strongest evidence yet that seaward shift of the  
560 fresh-saline interface induced by base-level fall can be a key control on sinkhole development.

In detail, the rates of shoreward migration of sinkhole development have been variable in space and time,  
and this may relate to other local or transient controls. The salt-rich evaporite materials may be  
anisotropically distributed through the subsurface in the study area (Polom et al., 2018). Focussing of  
565 groundwater into salt-rich ‘lenses’ in given years could explain the rapid development of new conduits at  
those times, hence leading to locally accelerated migration (**Figure 9**) and to jumps in the growth of the  
sinkhole population and of the uvalas, such as occurred in 2005 – 2006 and 2009 (**Figures 10 and 14**).  
Alternatively, or perhaps complementarily, such small-scale and short-term fluctuation in the  
spatiotemporal development of the sinkholes at Ghor al-Haditha may relate to variations in meteoric  
570 and/or groundwater inflow as inferred for several sinkhole sites on the western shore (Abelson et al.,  
2017).

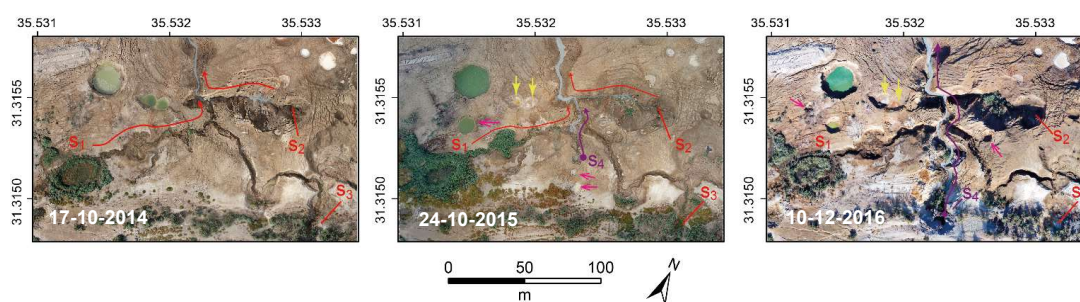
### 5.8 Links between surface stream flow, subsurface stream flow and sinkhole formation

Several features of the uvalas and the formation of sinkholes within them strongly suggest a link between  
their development and the channelized flow of groundwater. The best example of such links is seen at  
575 uvala U2 in association with the development of stream channel CM5 (**Figures 4, 12 and 16**). Firstly,  
CM5 developed from a spring, which emerged in the middle of the mudflat and in association with



drainage of a lake hosted in U2 (**Figure 4**). Secondly, the migration patterns of sinkholes within U2 converge at the spring location (**Figure 12**). Thirdly, upstream incision at the head of CM5 is spatially and temporally linked with sinkhole collapses (**Figure 16**), which occurred on a time-scale of a few days. 580 These collapses show that the water reaches the head of CM5 via subsurface conduits. Fourthly, U2 also hosts a vegetated pond (labelled  $s_1$  in **Figure 16**), which is fed by fresh non-sulphurous groundwater. This water therefore passes through the alluvial sediments without being significantly salinized by interstitial brine, indicated by low salinity ( $EC=20$  mS/cm) and light  $\delta^2H$  and  $\delta^{18}O$  signatures. These observations indicate the presence of subterranean channel flow, followed by surface flow and channel incision. 585 Therefore, in compliment to the arguments presented by Avni et al. (2016), the rapid development of sinkholes may not only occur due to ‘flash-flood’ style input, but also from steadier groundwater input.

Further evidence of such links is seen at Uvala U4, which is linked spatially and temporally with the spring feeding channel CM7 (the ‘black stream’) (**Figure 12**). Initial ground cracking at U4 occurred 590 proximal to a subtle linear depression (or ‘blind valley’) between it and the spring feeding the ‘black stream’, which is first observed in 2009. The migration of sinkholes within U4 seems to follow a flow path from the initial pre-uvuala sinkhole cluster to the ‘black stream’ head, suggesting the presence of a flow conduit beneath the depression. Additional ‘prongs’ of sinkhole migration and groundcracking at uvalas U4 and U3 (**Figures 12 and 13**) may also represent a surface expression of subsurface conduit development, although no associated springs have yet been observed. 595



600 **Figure 16:** Orthophotos of the canyon-spring-sinkhole system close to the former mud-factory at the head of CM5, displaying the evolution of surface water flow and sinkhole collapse and their links to subsurface flow. In 2014,  $s_1$  and  $s_2$  both feed downstream CM5. By 2015, a new spring,  $s_4$  has formed and cut back to the southeast, and carries more water than  $s_1$  and  $s_2$ . New sinkholes have formed nearby (green arrows). The formerly ponded sinkholes (labelled with yellow arrows) have dried considerably. By 2016,  $s_4$



carries all of the flow to CM5, and has back-eroded further. More new sinkholes have formed, and  $s_1$  and  $s_2$  are now totally dry. The spring that originally fed CM5, labelled  $s_3$ , has been dry since 2013.

605 These links between surface water, groundwater and sinkhole development show that the upper limit of subsurface karstification is variable across the study area but overall very shallow. Karstic development within the salt-rich deposits proximal to CM8 (**Figure 1**) was observed at less than a metre beneath the surface in the field (Al-Halbouni et al., 2017). Close to CM7 (the ‘black stream’), subsurface channelization must occur at a minimum depth of around -428 m (**Figure 12**) (the base of the adjacent uvala U4 is close to this elevation). Further south, evolution of CM5 and related sinkhole collapses  
610 shows that subsurface channelization occurred at less than 10m below the surface. The lower elevation limit of karstification is unknown but seismic and borehole data indicate that it locally must be at depths greater than 45 – 100 m (Polom et al., 2018).

615 Finally, the origins of the groundwaters driving the subsurface karstification and much of the surface channel development appear from our preliminary surveys to be sourced from all three of the adjacent aquifers (**Figures 2A and 15**). Sulphurous springs linked to sinkhole and uvala formation in the north of the area lie downslope of the Ram-Kurnub aquifer which is known to emit reducing sulphurous water (Charrach, 2018). In contrast, non-sulphurous springs are linked with sinkhole and uvala development in the south of the area, and are likely sourced from the adjacent Aljun and superficial gravel aquifers.

## 620 **5.9 Limitations and future work**

Much of the available data on the study area’s 50-year evolution is necessarily 2D in nature, as our 2014-2016 photogrammetric surveys were the first to yield 3D data at sufficient resolution. Additionally some of our analysis is necessarily qualitative in the absence of quantitative constraints on past stream discharge rates and groundwater levels. Future appraisal of the geomorphological evolution of this area and the related hazards ideally requires the following: (1) additional high-resolution and high-precision 3D  
625 topographical surveys, ideally at annual frequency or better; (2) monitoring of stream discharge and sediment load at high temporal resolution; (3) systematic drilling of boreholes to constrain subsurface lithologies, groundwater properties and groundwater levels.



## 6 Summary & Conclusions

630 Our results provide, for the first time in the study area, a detailed picture of the interlinked fluvial and karstic geomorphological responses of surface and subsurface hydrological systems to base level fall at the Dead Sea. Our main findings are as follows:

- 635 (1) The continuous and rapid fall in base level of the Dead Sea over the last 50 years has resulted in a number of geomorphological changes on the eastern shore, including: (i) incision of fluvial channels of atypical morphology into the former sea bed and into the marginal alluvial fan deposits; (ii) growth and progradation of new alluvial fans, (iii) formation of many sinkholes and several salt-karst uvalas.
- 640 (2) Channel morphologies in the former lakebed are V-shaped in cross-sectional profile and in plan-view can be divided in to meandering and straight types. Meandering channels show low W/D ratios (5-15) that are consistent along the longitudinal profile of the channel. These channels also show relatively low sinuosity (1.1 – 1.7). Straight channels show similar W/D ratios in their upper reaches but higher ratios (15-40) in their lower reaches, which are commonly braided. Channel morphology in the marginal alluvium is U-shaped (trapezoidal) in cross-section profile and straight in plan-view.
- 645 (3) The differences in channel morphology in the former lakebed are primarily related to differences in discharge and sediment load. Water in meandering channels is sourced from low-discharge groundwater springs and carries low-volume clay/silt dominated loads. Water in straight channels is probably sourced from flash-flood events traversing adjacent alluvial fans and carries higher volume loads of sand to cobble grade.
- 650 (4) Consistent with experimental studies, the relatively low sinuosity and low W/D of the channels in the former lakebed are compatible with a combination of the cohesive nature of the channel substrate and with a forcing by the continuous rapid base level fall. The factors inhibit lateral erosion and channel migration, and so vertical incision is the dominant response to base level fall.
- 655 (5) Over 1100 sinkholes have developed at Ghor al-Haditha since the mid-1980s. Rate of formation of sinkholes accelerated from the 1980s until 2009; since then a lower but steadier rate of formation (~60 holes per year). Sinkholes at Ghor al-Haditha form and grow in clusters. New clusters have initiated from SSW – NNE, roughly parallel to the modern shoreline.



- 660 (6) Sinkhole morphology is variable depending upon the material properties of the lithology in which they formed. Sinkholes formed in alluvium tend to have the highest  $D_e/D_i$  ratios (average 0.40), while those formed in mud-rich lacustrine deposits tend to have the lowest  $D_e/D_i$  ratios (average 0.09). Sinkholes formed in mud-rich lacustrine deposits can achieve much larger diameters than those in alluvium or salt-rich deposits.
- (7) Several salt-karst uvalas have developed around and in tandem with clusters of sinkholes. These uvalas are areas of subsidence several hundreds of metres in scale and in part bound systems of ground cracks and faults.
- 665 (8) The main geohazards arising from base level fall are fluvial erosion and sinkhole formation. Although there is still some risk to infrastructure in the more densely populated areas to the south, these hazards pose the greatest future risk to the infrastructure (Dead Sea highway) in the north of the study area.
- 670 (9) A progressive seaward migration in the development of the stream channels, alluvial fans, sinkholes and uvalas at Ghor al-Haditha ultimately reflect the underlying effect of base level fall on fluvial and karst systems. Seaward growth of channel and alluvial fans reflects incision into and deposition onto the progressively uncovered lakebed as the shore line retreats. Similarly, consistent seaward migration of sinkhole and uvala development may be linked to seaward propagation of a dissolution front, facilitated by lateral retreat of the fresh-saline interface at depth as the base level falls.

## 7 Data Availability

675 A full set of metadata is available upon request. Satellite images: some open access (Corona), but mostly commercial. Aerial images: available at discretion of RJGC. Photogrammetric surveys: raw images, DSMs and orthophotos available upon consultation with the authors. Geological Map 1:50,000 Ar Rabba: available at discretion of MEMR.

## 8 Author Contribution

680 RAW and EPH led the production of figures and writing of the manuscript. RAW undertook the majority of the data analysis associated with the satellite imagery time series and the 2015 and 2016 DSMs.



Additional satellite imagery processing and data analysis was performed by LS, DAH and EPH. DAH and LS generated the orthophotos and DSMs of the study area using SfM photogrammetry. EPH, DAH, LS, HAR, and AS undertook the field studies and close-range photogrammetric surveys in 2014 – 2016. 685 Water sampling was performed by EPH and LS in 2015, and isotopic analysis was overseen by CS. All authors reviewed and commented on the manuscript, and they contributed to discussions of the data.

## 9 Competing interests

The authors declare that they have no conflict of interest.

## 10 Special issue statement (will be included by Copernicus)

690

## 11 Acknowledgements

We acknowledge MEMR colleagues for support in fieldwork and other logistical support. The authors acknowledge financial support from GFZ and the Helmholtz Association's recent Dead Sea Research Venue (DESERVE) initiative (Kottmeier et al., 2016), especially for the associated data and fieldwork 695 costs. Part of the work of NAK was done during a sabbatical year supported by the Deanship of scientific research – The University of Jordan. RAW and EPH are also grateful to the Geological Survey of Ireland for providing funding for RAW's masters research project, of which this manuscript forms a central part.

## 12 References

Abelson, M., Baer, G., Shtivelman, V., Wachs, D., Raz, E., Crouvi, O., Kurzon, I. and Yechieli, Y.: 700 Collapse-sinkholes and radar interferometry reveal neotectonics concealed within the Dead Sea basin, *Geophys. Res. Lett.*, 30(10), 2–5, doi:10.1029/2003GL017103, 2003.  
Abelson, M., Yechieli, Y., Baer, G., Lapid, G., Behar, N., Calvo, R. and Rosensaft, M.: Natural versus human control on subsurface salt dissolution and development of thousands of sinkholes along the Dead



- Sea coast, *J. Geophys. Res. Earth Surf.*, 122(6), 1262–1277, doi:10.1002/2017JF004219, 2017.
- 705 Al-Halbouni, D., Holohan, E. P., Saberi, L., Alrshdan, H., Sawarieh, A., Closson, D., Walter, T. R. and Dahm, T.: Sinkholes, subsidence and subsrosion on the eastern shore of the Dead Sea as revealed by a close-range photogrammetric survey, *Geomorphology*, 285, 305–324, 2017.
- Al-Zoubi, A. and Ten Brink, U. S.: Salt diapirs in the Dead Sea basin and their relationship to Quaternary extensional tectonics, *Mar. Pet. Geol.*, 18, 779–797, 2001.
- 710 Allen, P. A.: From landscapes into geological history, *Nature*, 451(7176), 274–276, 2008.
- Asmar, B. N. and Ergenzinger, P.: Long-term prediction of the water level and salinity in the Dead Sea, *Hydrol. Process.*, 16(14), 2819–2831, doi:10.1002/hyp.1073, 2002.
- Avni, Y., Lensky, N., Dente, E., Shviro, M., Arav, R., Gavrieli, I., Yechieli, Y., Abelson, M., Lutzky, H., Filin, S., Haviv, I. and Baer, G.: Self-accelerated development of salt karst during flash floods along the
- 715 Dead Sea Coast, Israel, *J. Geophys. Res. Earth Surf.*, 121, 17–38, 2016.
- Bakalowicz, M.: Karst groundwater: A challenge for new resources, *Hydrogeol. J.*, 13(1), 148–160, 2005.
- Bartov, Y., Stein, M., Enzel, Y., Agnon, A. and Reches, Z.: Lake Levels and Sequence Stratigraphy of Lake Lisan, the Late Pleistocene Precursor of the Dead Sea, *Quat. Res.*, 57(01), 9–21, 2002.
- Best, J. L. and Ashworth, P. J.: Scour in large braided rivers and the recognition of sequence stratigraphic
- 720 boundaries [7], *Nature*, 387(6630), 275–277, doi:10.1038/387275a0, 1997.
- Bowman, D., Svoray, T., Devora, S., Shapira, I. and Laronne, J. B.: Extreme rates of channel incision and shape evolution in response to a continuous, rapid base-level fall, the Dead Sea, Israel, *Geomorphology*, (114), 227–237, doi:10.1016/j.geomorph.2009.07.004, 2010.
- Ten Brink, U. S. and Flores, C. H.: Geometry and subsidence history of the Dead Sea basin: A case for
- 725 fluid-induced mid-crustal shear zone?, *J. Geophys. Res.*, 117, doi:10.1029/2011JB008711, 2012.
- Buffington, J. and Montgomery, D.: Geomorphic classification of rivers, *Treatise Geomorphol.*, 9, 730–767, doi:10.1016/B978-0-12-374739-6.00263-3, 2013.
- Ćalić, J.: Karstic uvala revisited: Toward a redefinition of the term, *Geomorphology*, 134, 32–42, 2011.
- Charrach, J.: Investigations into the Holocene geology of the Dead Sea basin, *Carbonates and Evaporites*,
- 730 1–28, doi:10.1007/s13146-018-0454-x, 2018.
- Church, M.: Bed material transport and the morphology of alluvial river channels, *Annu. Rev. Earth*



- Planet. Sci., 34(1), 325–354, doi:10.1146/annurev.earth.33.092203.122721, 2006.
- Closson, D. and Karaki, N. A.: Salt karst and tectonics : sinkholes development along tension cracks between parallel strike-slip faults , Dead Sea , Jordan, *Earth Surf. Process. Landforms* , 34(June), 1408–735 1421, doi:10.1002/esp, 2009.
- Closson, D., Abou Karaki, N. and Hallot, F.: Landslides along the Jordanian Dead Sea coast triggered by the lake level lowering, *Environ. Earth Sci.*, 59(7), 1417–1430, doi:10.1007/s12665-009-0128-z, 2010.
- Dansgaard, W.: Stable isotopes in precipitation, *Tellus*, 16(4), 436–468, 1964.
- Davis, W. M.: Base level, grade and peneplain, *J. Geol.*, 10, 77–111, 1902.
- 740 Ebisa Fola, M. and Rennie, C. D.: Downstream Hydraulic Geometry of Clay-Dominated Cohesive Bed Rivers, *J. Hydraul. Eng.*, 136(8), 524–527, doi:10.1061/(ASCE)HY.1943-7900.0000199, 2010.
- El-Isa, Z., Rimawi, O., Jarrar, G., Abou Karaki, N., Taqieddin, S., Atallah, M., Seif El-Din, N. and Al Saed, E.: Assessment of the Hazard of Sinkholes and Subsidence in the Ghor al-Haditha Area, Amman, Jordan., 1995.
- 745 Epstein, S. and Mayeda, T.: Variation of O18 content of waters from natural sources, *Geochim. Cosmochim. Acta*, 4(5), 213–224, doi:10.1016/0016-7037(53)90051-9, 1953.
- Ezersky, M. G., Eppelbaum, L. V., Al-Zoubi, A., Keydar, S., Abueladas, A., Akkawi, E. and Medvedev, B.: Geophysical prediction and following development sinkholes in two Dead Sea areas, Israel and Jordan, *Environ. Earth Sci.*, 70(4), 1463–1478, doi:10.1007/s12665-013-2233-2, 2013.
- 750 Farrant, A. R. and Simms, M. J.: Ogof Draenen: Speleogenesis of a hydrological see-saw from the karst of South Wales, *Cave Karst Sci.*, 38(1), 31–52, 2011.
- Fiaschi, S., Closson, D., Abou Karaki, N., Pasquali, P., Riccardi, P. and Floris, M.: The complex karst dynamics of the Lisan Peninsula revealed by 25 years of DInSAR observations. Dead Sea, Jordan, *ISPRS J. Photogramm. Remote Sens.*, 130, 358–369, doi:10.1016/j.isprsjprs.2017.06.008, 2017.
- 755 Filin, S., Baruch, A., Avni, Y. and Marco, S.: Sinkhole characterization in the Dead Sea area using airborne laser scanning, , 1135–1154, doi:10.1007/s11069-011-9718-7, 2011.
- Ford, D. and Williams, P.: *Karst Hydrogeology and Geomorphology*, edited by D. Ford and P. Williams, Wiley, Chichester., 2007.
- Garfunkel, Z. and Ben-Avraham, Z.: The structure of the Dead Sea basin, *Tectonophysics*, 266(1–4),



- 760 155–176, doi:10.1016/S0040-1951(96)00188-6, 1996.
- Gat, J. R. and Dansgaard, W.: Stable isotope survey of the fresh water occurrences in Israel and the northern Jordan rift valley, *J. Hydrol.*, 16, 177–211, 1972.
- Gutiérrez, F., Parise, M., De Waele, J. and Jourde, H.: A review on natural and human-induced geohazards and impacts in karst, *Earth-Science Rev.*, 138, 61–88, doi:10.1016/j.earscirev.2014.08.002, 2014.
- 765 John E. Koss, Frank G. Ethridge, S., J. E., Ethridge, F. G. and Schumm, S. A.: An Experimental Study of the Effects of Base-Level Change on Fluvial, Coastal Plain and Shelf Systems, *SEPM J. Sediment. Res.*, Vol. 64B(2b), 90–98, doi:10.1306/D4267F64-2B26-11D7-8648000102C1865D, 1994.
- Khalil, B.: The Geology of the Ar Rabba area, Map Sheet No 3125 IV, Bull 22, Amman, Jordan., 1992.
- Kottmeier, C., Agnon, A., Al-halbouni, D., Alpert, P., Corsmeier, U., Dahm, T., Eshel, A., Geyer, S.,
- 770 Haas, M., Holohan, E., Kalthoff, N., Kishcha, P., Krawczyk, C., Lati, J., Laronne, J. B., Lott, F., Mallast, U., Merz, R., Metzger, J., Mohsen, A., Morin, E., Nied, M., Rödiger, T., Salameh, E., Sawarieh, A., Shannak, B., Siebert, C. and Weber, M.: New perspectives on interdisciplinary earth science at the Dead Sea : The DESERVE project, *Sci. Total Environ.*, 544(December 2015), 1045–1058, 2016.
- Kranjc, A.: Classification of Closed Depressions in Carbonate Karst, in *Treatise on Geomorphology*,
- 775 Volume 6, edited by A. Frumkin, pp. 104–111, Academic Press, San Diego, CA, San Diego., 2013.
- Lensky, N. G., Dvorkin, Y., Lyakhovskiy, V., Gertman, I. and Gavrieli, I.: Water, salt, and energy balances of the Dead Sea, *Water Resour. Res.*, 41(12), doi:10.1029/2005WR004084, 2005.
- Leopold, L. B. and Bull, W. B.: Base Level, Aggradation, and Grade, *Proc. Am. Philos. Soc.*, 123, 168–202, doi:10.2307/986220, 1979.
- 780 Leopold, L. B. and Wolman, M. G.: River channel patterns: braided, meandering, and straight, US Government Printing Office., 1957.
- Lowe, D. and Waltham, T.: A dictionary of karst and caves. Cave Studies Series, 6, British Cave Research Association, London., 1995.
- M. Gehre, \*, R. Hoefling, P. Kowski, and and Strauch, G.: Sample Preparation Device for Quantitative
- 785 Hydrogen Isotope Analysis Using Chromium Metal, *Anal. Chem.*, 68(24), 4414–4417, 1996.
- Moshe, L. Ben, Haviv, I., Enzel, Y., Zilberman, E. and Matmon, A.: Incision of alluvial channels in response to a continuous base level fall: Field characterization, modeling, and validation along the Dead



- Sea, *Geomorphology*, 93, 524–536, doi:10.1016/j.geomorph.2007.03.014, 2008.
- 790 Peakall, J., Ashworth, P. J. and Best, J. L.: Meander-Bend Evolution, Alluvial Architecture, and the Role  
of Cohesion in Sinuous River Channels: A Flume Study, *J. Sediment. Res.*, 77(3), 197–212,  
doi:10.2110/jsr.2007.017, 2007.
- Polom, U., Alrshdan, H., Al-Halbouni, D., Holohan, E. P., Dahm, T., Sawarieh, A., Atallah, M. Y. and  
Krawczyk, C. M.: Shear wave reflection seismic yields subsurface dissolution and subsrosion patterns:  
application to the Ghor Al-Haditha sinkhole site, Dead Sea, Jordan, *Solid Earth*, 9, 1079–1098,  
795 doi:10.5194/se-9-1079-2018, 2018.
- Salameh, E. and El-Naser, H.: Changes in the Dead Sea Level and their Impacts on the Surrounding  
Groundwater Bodies, *Acta Hydrochim. Hydrobiol.*, 28(1), 24–33, doi:10.1002/(SICI)1521-  
401X(200001)28:1<24::AID-AHEH24>3.0.CO;2-6, 2000.
- Sawarieh, A., Al Addas, A., Al Bashish, M. and Al Seba'i, E.: Sinkholes Phenomena At Ghor Al Haditha  
800 Study Area.- Internal Report No. 12, Amman, Jordan., 2000.
- Schumm, S. A.: River Response to Baselevel Change: Implications for Sequence Stratigraphy, *J. Geol.*,  
101, 279–294, 1993.
- Schumm, S. A. and Khan, H. R.: Experimental Study of Channel Patterns, *Geol. Soc. Am. Bull.*, 83,  
1755–1770, 1972.
- 805 Shalev, E. and Lyakhovskiy, V.: Viscoelastic damage modeling of sinkhole formation, *J. Struct. Geol.*,  
42, 163–170, doi:10.1016/j.jsg.2012.05.010, 2012.
- Siebert, C., Rödiger, T., Mallast, U., Gräbe, A., Guttman, J., Laronne, J. B., Storz-Peretz, Y., Greenman,  
A., Salameh, E., Al-Raggad, M., Vachtman, D., Zvi, A. Ben, Ionescu, D., Brenner, A., Merz, R. and  
Geyer, S.: Challenges to estimate surface- and groundwater flow in arid regions: The Dead Sea catchment,  
810 *Sci. Total Environ.*, 485–486, 828–841, doi:10.1016/J.SCITOTENV.2014.04.010, 2014.
- Simon, A. and Darby, S. E.: Process-form interactions in unstable sand-bed river channels: A numerical  
modeling approach, *Geomorphology*, 21(2), 85–106, doi:10.1016/S0169-555X(97)00043-3, 1997.
- Torfstein, A., Haase-Schramm, A., Waldmann, N., Kolodny, Y. and Stein, M.: U-series and oxygen  
isotope chronology of the mid-Pleistocene Lake Amora (Dead Sea basin), *Geochim. Cosmochim. Acta*,  
815 73(9), 2603–2630, doi:10.1016/J.GCA.2009.02.010, 2009.



- Vachtman, D. and Laronne, J. B.: Hydraulic geometry of cohesive channels undergoing base level drop, *Geomorphology*, 197, 76–84, doi:10.1016/j.geomorph.2013.04.039, 2013.
- Whittaker, A. C.: How do landscapes record tectonics and climate?, *Lithosphere*, 4(2), 160–164, 2012.
- Whittaker, A. C. and Boulton, S. J.: Tectonic and climatic controls on knickpoint retreat rates and  
820 landscape response times, *J. Geophys. Res. Earth Surf.*, 117(2), 1–19, doi:10.1029/2011JF002157, 2012.
- Yechieli, Y.: Fresh-Saline Ground Water Interface in the Western Dead Sea Area, *Ground Water*, 38(4), 615–623, doi:10.1111/j.1745-6584.2000.tb00253.x, 2000.
- Yechieli, Y. and Gavrieli, I.: Will the Dead Sea die?, *Geology*, 26(8), 755–758, doi:10.1130/0091-7613(1998)026<0755:WTSDSD>2.3.CO;2, 1998.
- 825 Yechieli, Y., Abelson, M., Bein, A., Crouvi, O. and Shtivelman, V.: Sinkhole “swarms” along the Dead Sea coast: Reflection of disturbance of lake and adjacent groundwater systems, *Bull. Geol. Soc. Am.*, 118(9–10), 1075–1087, doi:10.1130/B25880.1, 2006.
- Yechieli, Y., Kafri, U., Wollman, S., Shalev, E. and Lyakhovsky, V.: The effect of base level changes and geological structures on the location of the groundwater divide, as exhibited in the hydrological  
830 system between the Dead Sea and the Mediterranean Sea, *J. Hydrol.*, 378(3–4), 218–229, 2009.
- Yechieli, Y., Abelson, M. and Baer, G.: Sinkhole formation and subsidence along the Dead Sea coast, Israel, *Hydrogeol. J.*, 24(3), 601–612, doi:10.1007/s10040-015-1338-y, 2016.
- Yoxall, W. H.: The Relationship between Falling Base Level and Lateral Erosion in Experimental Studies, *Geol. Soc. Am. Bull.*, 80, 1379–1384, 1969.